DRIVERS OF GROUNDWATER FLOW AT A BACK BARRIER ISLAND – MARSH TRANSECT IN COASTAL GEORGIA

by

JONATHAN GREGORY LEDOUX

(Under the Direction of Christof Meile)

ABSTRACT

The tidal marsh connects terrestrial landscapes with the coastal ocean. Groundwater within this environment has the ability to move nutrients and influence plant distribution. Land-use change and Sea Level Rise (SLR) threaten to change these groundwater patterns. Monitoring wells recording conductivity, temperature, and water level across a back barrier island-marsh transect at Sapelo Island, GA, identified drivers of groundwater flow. Pressure propagation from tidal variations in creek water level was negligible at the study site. Density-driven flow had little impact on groundwater movement. The saturated nature of the marsh allowed for the well nearest the tidal creek to be used as an inundation meter, and the effect of tidal flooding was identified using three different techniques. Filtering the tidal signal record demonstrated that precipitation, was a main factor for water level changes in the well nearest the upland.

INDEX WORDS: Groundwater, Sapelo Island, Slug Test, Density Driven Flow, Precipitation, Cross Correlation, CTD Sonde, Darcy Velocities

DRIVERS OF GROUNDWATER FLOW AT A BACK BARRIER ISLAND – MARSH TRANSECT IN COASTAL GEORGIA

by

JONATHAN GREGORY LEDOUX

B.S., Coastal Carolina University, 2011

A Thesis Submitted to the Graduate Faculty of The University of Georgia in Partial Fulfillment of the Requirements for the Degree

Master of Science

Athens, Georgia

2015

DRIVERS OF GROUNDWATER FLOW AT A BACK BARRIER ISLAND – MARSH TRANSECT IN COASTAL GEORGIA

by

JONATHAN GREGORY LEDOUX

Major Professor: Christof Meile

Committee: Todd Rasmussen

Clark Alexander

Electronic Version Approved:

Suzanne Barbour
Dean of the Graduate School
The University of Georgia
August 2015

ACKNOWLEDGEMENTS

I would like to thank my committee members, Todd Rasmussen and Clark Alexander, for being flexible and always willing to help when needed and having the patience to see me through to the end. I would like to thank my primary advisor, Christof Meile, for always giving me the necessary support and time to succeed. I would not be here without his tough love and encouragement throughout my time in the lab.

I would like to thank the technicians, especially Jacob Shalack and Caroline Reddy, who spent many hours in the heat and cold during the hour and a half boat ride one way and twenty minute walk through the marsh to collect my data. Thank you to Clark Alexander and those involved in installing the piezometers and collecting the vibracores. I would like to thank the GCE-LTER and the marine science department for funding my project efforts.

I would like to thank my lab mates; Eric King, Maggie Esch, Kathy Loftis, David Miklesh, Tommy Dornhoffer, and Jurjen Rooze. A big thanks to my friends in the department pushing me and supporting me; Charles Schutte, Jonathan Taylor, Christian Edwards, Jared Mcknight, Michael Seidel, Annette Hynes, and Anna Tansik.

To my family, especially my mother and father, for supporting me through all the good and bad times of graduate school, your unwavering support gave me the strength to achieve my goals. I have not traveled this journey alone, a huge thanks goes to my best friends and roommates, Mark Jones, Mellissa Roskosky, and Sara Hiers for being there with encouragement, wisdom, or a beer when I needed it.

TABLE OF CONTENTS

Page

LIST OF TABLES

Page

LIST OF FIGURES

Page

CHAPTER 1

INTRODUCTION

Importance of Salt Marshes

Coastal salt marshes act as a buffer between terrestrial and marine ecosystems, connecting coastal cities and the ocean. These salt marshes are home to many species year round and are vital breeding grounds for migratory birds and other marine organisms (Hackney et al. 1976; Odum 1988; Wenner and Betty 1993; Isacch et al 2004). Maintaining the stability of these environments is important as marshes can remove dissolved chemical constituents (Boorman 1999; Cacador and Vale 2001; Huang and Pant 2009). This process has long been recognized and employed in wastewater treatment of both surface flows (river, runoff) and groundwater (Hammer 1992; Comin et al. 1997; Crities et al. 2006). The ability to remove anthropogenic pollutants can help maintain the health of the coastal seas by reducing eutrophication. Additional metals, such as Pb and Cd (Alexander et al. 1993), and nutrient loading (Gedan et al. 2009) are seen enriched in the marsh over time as coastal populations increase.

The Georgia coast consists of 8 clusters of barrier islands protecting the mainland from the sea and tidal forcings (Johnson and Barbour 1990). The powerful force of the tide has the ability to change coastal environments through sediment transport (Christiansen et al. 1999); the marshes are always changing morphologically (Edwards et al. 2004). The large tidal forcing can be seen in sinusoidal variations in the

water table, extending the influence beyond the beach and tidal creeks at the beach face (Nielsen 1990; Schultz and Ruppel 2002). The stability of these ecosystems can be easily affected by elevation relative to sea level due to erosion (Stevenson et al. 1985).

Groundwater at the Coast

It is important to consider the role of groundwater at the coast because it can influence the distribution of vegetation (Ursino et al., 2004) and can be responsible for a potentially large fraction of nutrient fluxes to the coastal ocean (Swarzenski et al., 2007). While marshes can effectively remove bioavailable N through denitrification, marsh porewaters are characterized by high concentrations of nutrients due to the break down of organic matter within the marsh. Submarine groundwater discharge (SGD) is a body of water, consisting a mixture of fresh, brackish and/or marine inputs, entering the coastal waters through the subsurface, including re-circulated sea water (Burnett et al. 2003). SGD is considered one of the many mechanics that can lead to the degradation of the coastal ocean by increasing nutrients resulting in eutrophication (McCoy et al. 2011). The groundwater beneath barrier islands is fresh, with salinities near 0, while the water regularly inundating the marsh is near 35. These two distinct water bodies can mix beneath the marsh or barrier island and form brackish waters. Due to evapotranspiration, salinity can exceed that of the inundating ocean water.

Certain vegetation species are able to tolerate high salinity environments (Mendelssohn and Morris 2000). The vegetation serves as a food source (Deegan and Garritt 1997), a habitat for marsh organisms (Bellis 1995), and helps stabilize the marsh from erosion (Callaway et al. 1997; Hughes 2001; Silva and Cacador 2009). Vegetation zonation has been highly studied within the salt marsh (e.g., Chapman 1974; Vince and

Snow 1984; Pennings & Callaway 1992). Several factors control the distribution of vegetation, and one of the main controlling determinants is salinity (Clarke and Hannon 1970; Cooper 1982).

In a salt marsh environment, there are several drivers of groundwater flow. On the rising tide, a pressure wave is propagated through the subsurface of the marsh, influencing groundwater flow (Schultz & Ruppel 2002). Differences in fluid temperature and salinity give rise to density-driven flow (Schincariol et al. 1994). In addition, high temperatures can cause significant evaporation across the marsh, and salinities in salt pans can reach 60 during parts of the year (Hughes et al. 2012), potentially inducing salt fingering (Diersch and Kolditz 2002; Shen et al. 2015). Groundwater discharge occurs when the tidal creek water levels fall below the water levels in the surrounding marsh. Finally, wind and low-pressure systems can alter the ocean water level, thereby affecting pressure gradients in surficial aquifers (Balugani and Antonellini 2011).

Threats to Current Conditions

Quantifying the different drivers of groundwater flow can help predict future changes in groundwater dynamics due to urbanization and land use change or climate change. Together these two factors have the ability to completely change the southeast US coasts within the next century (Morzaria-Luna et al. 2014). The southeast has the fastest growing population of all the coastal regions (Crossett et al. 2004). As this growth occurs, the increase in developed property will likely degrade the salt marshes (Bertness et al. 2001). Humans impact the marsh by creating sea walls, docks, and levees, which all directly destroy marsh habitat (Kennish 2001).

One of the main impacts of climate change is sea level rise (SLR) (Church et al. 2001). Much research has gone into estimating the impact of SLR on coastal populations (Miller and Douglas 2004; Douglas and Peltier 2002; Zhang and Gorelick 2014). Ericson et al. (2006) suggest that by the year 2050 approximately 8.7 million people within deltas worldwide would be affected by accelerated erosion and an increase in inundation distances onto the coast. However before coastal populations are impacted, SLR will alter the barrier islands and the surrounding marshes. Craft et al. (2009) predicted that SLR could cause up to 45% of salt marshes to decline from present day amounts due to inundation. The rate of relative sea level rise and the local vegetation will determine how each individual marsh is affected (Morris et al. 2002). If sediment accretion is unable to keep up, SLR will not only drown a marsh, but it may also alter groundwater flow patterns (Blum and Roberts 2009). Sea level rise has the ability to reduce or reverse regional hydraulic gradients causing salt-water intrusion to occur (Uddameri et al. 2014). Due to the threat of loss of water resources, research has started to focus on the interactions between groundwater and climate change (Werner and Simmons 2009; Guha and Panday 2012; Loaiciga et al. 2012). Climate change will affect coastal salt marshes not only by SLR but also by a change in atmospheric and weather patterns (Doney et al. 2012).

Purpose of the Study

This study utilizes shallow piezometer wells instrumented with conductivity, temperature, and depth probes (CTD) to identify the influence of different drivers of groundwater flow. Previous studies mainly focused on the impact that the tide has on groundwater flow, mostly conducted through the use of models (Ursino et al. 2003;

Gardner 2005; Gardner 2005; Li et al. 2005; Marani et al. 2006; Wilson and Gardner 2006; Yuan et al. 2011), or the impact of density gradients (Smith 2004). Modeling groundwater flow through the marsh domain can be very difficult due to the numerous changing variables at any given time (Quintana et al. 2006). This study includes all the drivers of groundwater flow using both models and field-measured data. Through manipulating Darcy's law, implementing tools used by oceanographers to quantify tidal forcing, and different statistical analyses we are able to assess groundwater flow in the upland-creek transition and look at the impacts of each driver of groundwater flow.

CHAPTER 2

METHODS

Study Site

The study site is located on the small hammock (back barrier island) Hn_i_1, formed during the Holocene (Turck and Alexander 2013), on the west side of Blackbeard Island on the Georgia coast (Figure 1) at 31.51881° N and 81.20945° W. - The hammock is roughly 215 meters long by 15 meters wide. The marsh surrounding the hammock is inundated by a semi-diurnal tide. Vibracores were collected and analyzed along a marsh transect (Figure 2) in 2008 by C. Alexander. The vibracores reached depths between 2.5 and 4.5 meters below the surface. Measurements such as grain size, % sand, silt, and clay, as well as core stratigraphy were taken. The transect from well 1 to well 8 is roughly 130 meters in length.

Hydrogeological Data

As part of the Georgia Coastal Ecosystems – Long Term Ecological Research (GCE – LTER) project, shallow PVC piezometers were installed on October 30th, 2008, spanning from Blackbeard Island, across a hammock and out toward a tidal creek (Figure 2). Locations were chosen to include each dynamic environment (upland, back marsh, hammock, and creek-ward marsh) and the transition zones captured by the transect to get a complete idea of how the groundwater patterns change and respond over time and space. To acquire the piezometer depth below the surface, the total length of the PVC well casing was subtracted from the length of the well protruding out

of the marsh. The depth of each well varied from 0.99 m to 2.38 m from the ground surface to the bottom of the well. Each piezometer has a thinly screened section, which extends 0.3 m from the bottom of the wells, and is located in the sandy surficial aquifer. This allows groundwater from that section to flow freely in and out of the piezometer while not allowing sediment through. A CTD sonde (Schlumberger CTD-Diver) was attached to the top of the piezometer and left to hang approximately 0.25 meters from the bottom of the well. The red dots in Figure 2 show the location of each CTD-Diver. All the sensors were placed in the surficial aquifer, above the confining mud layer. CTD loggers from August 25th, 2011 to June 27th, 2012 recorded the data every 15 minutes.

Data Treatment

The atmospheric pressure was subtracted from the raw pressure data recorded inside the piezometers (Rasmussen and Crawford 1997). Pressure records from the Marsh Landing meteorological monitoring station was downloaded from the GCE-LTER website to perform the corrections. Well water densities were calculated using UNESCO algorithms (UNESCO 1982) based on the measured salinity and temperature in the well. Water levels were calculated using the equation:

$$H = \frac{P}{\rho g} \quad (1)$$

where H is water height, P is pressure, ρ is density, and g is gravity.

When the piezometers were installed, elevations of the well locations were recorded using a real time kinematic (RTK) GPS receiver. The elevation of each well was recorded relative to the NAVD88 datum. This allows all the wells and the associated CTD sonde to be compared to the same elevation point. The water height

from equation 1 can then be converted into a water level that is referenced to the same NAVD88 datum using the values in Table 1.

$$SG = DW - B - T \quad (2)$$

where SG is water level above the sensor, DW is entire length of the piezometer pipe, B is sensor distance from well bottom, and T is ground to well top.

Before identifying horizontal flow patterns from pressure differences between wells, the sensors must be referenced to the same elevation. Here, the average sensor elevation across all wells was chosen, rather than NAVD88. This reduced the amount of error that could occur due to vertical salinity changes. We chose to keep salinity as the measured value as the elevation corrections between the actual CTD elevation and the referenced elevation were small.

When all the water levels were referenced to the same depth, it was seen that the peak water height during inundation for well 7 was consistently higher than in the other wells. To quantify this systematic offset, the peaks during tidal inundation were identified for both wells 7 and 8. Peaks that did not co-occur within a tidal cycle at both wells were removed. The remaining paired peaks were then compared against each other to quantify a systematic offset between the ground-elevation of well 7.

Darcy's Law and the Decomposition of Pressure Signals

Groundwater flow depends on properties of the porous media, the fluid and the pressure gradient. In one dimension, flow along the x-axis can be expressed as (Bear 1972):

$$\mathrm{q} = -\frac{\mathrm{k}}{\mu} * \frac{\partial \mathrm{P}}{\partial x} \quad (3)$$

where q is the Darcy flow velocity (m/s), k is the intrinsic permeability (m^2), μ is the dynamic viscosity (Ns/m^2), and $\frac{\partial P}{\partial x}$ is the horizontal pressure gradient (N/m^3). The measured pressure (P^m) can be broken into two different components, separating the effect of density variations on pressure (P^d) from piezometric head (P^h)

$$P^m = P^h + P^d \tag{4}$$

Pressure can be expressed as

$$P = \rho g h \tag{5}$$

where ρ is density (kg/m^3), h denotes the head (m) and g is gravitational acceleration (m/s^2). One can decompose both the head and the density into a reference head and density (h_{avg}, ρ_{avg}) and a deviation from it (h', ρ'), respectively, so that

$$P = (\rho_{avg} + \rho')g(h_{avg} + h') \tag{6}$$

The pressure gradient can then be written as:

$$\frac{\Delta P^m}{\Delta x} = \frac{\left((\rho_{avg}+\rho'_{i+1})g(h_{avg}+h'_{i+1})\right)}{x_{i+1}-x_i} - \frac{((\rho_{avg}+\rho'_i)g(h_{avg}+h'_i))}{x_{i+1}-x_i} \tag{7}$$

where the subscripts i and i+1 denote two adjacent wells. Multiplying through and cancelling results in:

$$\frac{\Delta P^m}{\Delta x} = \frac{\left(\rho_{avg}g(h'_{i+1}-h'_i)\right)}{x_{i+1}-x_i} + \frac{\left(h_{avg}g(\rho'_{i+1}-\rho'_i)\right)}{x_{i+1}-x_i} + \frac{(g(\rho'_{i+1}h'_{i+1}-\rho'_i h'_i))}{x_{i+1}-x_i} \tag{8}$$

Choosing the reference density and head to be the average between two adjacent wells, the deviations (y' = y - y_{avg}) for head (h') and pressure (p') can be written as

$$h'_{i+1} = -h'_i = \frac{\Delta h}{2} \tag{9}$$

$$\rho'_{i+1} = -\rho'_i = \frac{\Delta \rho}{2} \tag{10}$$

which results in

$$\frac{\Delta P^{m}}{\Delta x} = \frac{(\rho_{avg} g \Delta h)}{x_{i+1} - x_i} + \frac{(h_{avg} g \Delta \rho)}{x_{i+1} - x_i} \quad (11)$$

Hence, we identify the piezometric pressure gradient as

$$\frac{\Delta P^{h}}{\Delta x} = \frac{(\rho_{avg} g \Delta h)}{x_{i+1} - x_i} \quad (12)$$

and the density-driven flow component as

$$\frac{\Delta P^{s}}{\Delta x} = \frac{(h_{avg} g \Delta \rho)}{x_{i+1} - x_i} \quad (13)$$

Slug Test

To determine the soil hydraulic conductivity, a slug test was conducted, in which water was either quickly added or removed and the response of pressure or water level is recorded. This response reflects the characteristics of the local aquifer. Four wells were selected for the slug test: Wells 1 & 8, to identify the properties of the aquifer closest to the tidal creek and the barrier island, respectively, well 5, representing the aquifer characteristics of the hammock, and well 3, located in the tidal marsh between the barrier island and the hammock.

To conduct the slug test, 600 mL of water was instantaneously added to a well. With a well diameter of 5 cm, this resulted in a predicted water height change of 30.6 cm, which makes the response of the well head easily measurable. A HOBO pressure sensor was used to measure the response in the wells. The sensor was set to record every 5 seconds. Prior to water being added, the well was pumped to remove any sediment that may have settled in the well and allowed to recover for at least 20 minutes. Coinciding with the well being pumped, 600 mL of the water was kept to conduct the tests, to prevent density change error.

In order to calculate hydraulic conductivity from the pressure sensors, the following mathematical equation was used (Freeze & Cherry 1979):

$$K = \frac{r^2 \ln(\frac{L}{R})}{2LT_0} \quad (14)$$

where *K* is hydraulic conductivity, *r* is the radius of the well, *L* is the length of the screened well section, *R* is the radius of the screened section, and T_0, the basic time lag, is graphically measured from the logarithmic decay of the water level using the data collected from when the slug was added to another point at least after a minute has passed. This equation takes into account the well diameter and the logarithmic nature of the pressure decay directly after the slug was added.

Subsurface Pressure Wave Propagation

As the flood tide rises in the tidal creek, the pressure associated with the rising water mass will be exerted upon the creek bank. This pressure is then felt for a certain distance across the marsh, propagating in the form of a pressure wave (Figure 3). Depending on the marsh characteristics, this pressure wave can be measureable for a long distance. The response of the pressure wave from the tidal creek can be modeled by (Schultz and Ruppel 2002):

$$h(x,t) = b + \sum_{j=1}^{\omega_N} A_j \exp\left[-x\sqrt{\frac{\omega_j}{2D}}\right] \cos\left(\omega_j t - \Phi_j - x\sqrt{\frac{\omega_j}{2D}}\right) \quad (15)$$

where *A, ω,* and *Φ* describe the tidal signal typical for the study site, *D* is diffusivity set to 0.0048 $m^2\ s^{-1}$, calculated as D=K*b/S where b is the average saturated thickness set to 1.5 m, K the hydraulic conductivity of 2.3 $*10^{-5}$ m/s, determined by slug test at well 8, and S is storativity, set to 0.2 (Schultz & Ruppel 2002). The tidal signal that was input

into the model was a simple sinusoidal signal with a tidal height of 0.75 m, which is a representative tidal height of a back barrier island and marsh at Sapelo Island.

Dominant Modes in the Signal

The remaining drivers for groundwater flow were investigated using various signal analysis and statistical tools. Tidal frequency fitting is often used by oceanographers to identify and remove the tidal frequencies within any signal. Empirical mode decomposition (EMD) breaks any signal into a series of modes by identifying peaks and troughs in the signal. Subsequently, a Fast Fourier Transform was performed in attempt to identify tidal frequencies. In addition, an Empirical Orthogonal Function examines the transect over both space a time, which allows the identification of different forcing patterns along a transect.

Matching Time Series With Signals Of Known Tidal Frequencies

One method used to attempt to remove tidal influences from the raw water level signal was using harmonic analysis. The matlab package U_Tide (Codiga 2011) associates known tidal frequencies with the pressure time series. It determines amplitude and lag for 59 tidal constituents. U_Tide computes a Signal to Noise Ratio (SNR) with each constituent (Codiga 2011) and identifies and omits constituents that cannot clearly be distinguished from noise. When the SNR has a value greater than two, that constituent is deemed significantly important. The water level from each well was input into U_Tide. Additional inputs into U_Tide include the latitude (32 deg N), ‘auto’ to specify which constituents to identify, ‘NodsatNone’ to omit satellite corrections, ‘White’ to use a white floor assumption with confidence intervals, ‘Ols’ which utilizes an

ordinary least squares method, and lastly 'LinCI' which implements a linearized method to determine confidence intervals. See appendix for matlab code.

Fast Fourier Transform

In attempt to acquire frequencies of tidal inundation, a Fast Fourier Transform (FFT) was implemented. This analysis uses an algorithm to take a complex signal, consisting of many sinusoidal signals, and break the signal into the individual frequencies (Cooley & Tukey 1965). Associated with each individual frequency is an amplitude and a phase shift. The pressure time series is input into the FFT function of matlab and the relevant frequencies and their associated amplitudes are visualized using stem plots (see appendix).

Empirical Mode Decomposition

A mathematically robust way to examine the signals across the marsh is to use an Empirical Mode Decomposition, as this approach does not require the signal to be composed of sinusoidal functions, which may constrain the applicability of an FFT to identifying non-sinusoidal signals (Wang et al. 2012). EMD systematically breaks down a complete signal into individual modes or functions, which when summed together represent the original signal. To be able to do this, EMD first fits a signal through the peaks of the input signal. The second step of EMD is to fit a second signal through the troughs of the input signal. The two signals are summed together to acquire the first mode. That mode is then removed from the original signal. This process is then repeated until the remaining signal becomes monotonic, where no additional modes can be extracted (Huang et al. 1998). An adapted script for use in matlab from Torres et al. (2011) was used to conduct an EMD on the water level at well 8. A noise standard

deviation of 0.05 was used in order to properly identify the peaks and troughs of the signal rather than identifying the noise in the signal. The small noise standard deviation was chosen due to the high quality of the data being used. Additional inputs include a number of realizations at 100 and a maximum number of sifting iterations allowed of 10. Once the EMD was conducted, FFT was run on each mode to identify periodic signals.

Empirical Orthogonal Function

Different functions can be identified using a version of a Principle Component Analysis (PCA) called Empirical Orthogonal Function (EOF). A script based on an implementation by Renato Castelao was used to perform an EOF analysis on the water level signals of each well. The input for EOF consists of a matrix where the rows are the water levels over time and the columns represent each well. The matrix was then de-trended by removing the average for each well. EOF uses a singular value decomposition (svd) to break the matrix into three separate matrixes. One of the matrixes from the svd is the eigenvalues of the input matrix. Each eigenvalue from EOF is divided by the total sum of all the eigenvalues and multiplied by 100 to see the percent variance for each function. After the percent variance was calculated, the top contributing functions were run through FFT to see the contributing frequencies associated with these respective functions.

Inundation Meter

Due to the geomorphology and the saturation level of the salt marsh, well 8, the piezometer closest to the tidal creek, can be used as an inundation meter. The flooding tide is measureable as it over tops the marsh. When the inundation water level drops below the marsh during an ebbing tide, the water level in the marsh does no drop below

ground elevation. The signal is non-sinusoidal with the water level rarely dropping below the saturated marsh water level. Each flooding tide that inundates the marsh has a very similar rate of increasing water level. A combination of the predictable rise of a flooding tide and the marsh being fully saturated allows the start of tide to be identified. A threshold value for the change of water level between two points of $5.9*10^{-3}$ m/0.25 hr was visually identified as an indicator of tidal inundation. When the change in water level reaches the threshold, the marsh is considered to become inundated and the timing of this event is recorded. This results in a time window, between the start of the first inundation event to just before the second event, during which the marsh has a flooding tide, an ebbing tide, and a period in which it is not inundated. The first time point, once the threshold is exceeded, is stored as the time of inundation for each tidal cycle.

To remove the remaining influence of tidal inundation due to pressure gradients from the surrounding marsh, three methods were utilized. Method 1 implemented the same technique as described above, using the same threshold of $5.9*10^{-3}$ m/0.25 hr. This same technique can be implemented again because the remaining tidal influence has the same characteristics as the raw water level. The second method was to identify minima in the inundation-removed signal, attributing low peaks to the base flow. The last method was to run a Butterworth low pass filter to remove semi-diurnal and higher frequencies from the corrected water table time series. The cutoff frequency was $2.48*10^{-5}$ Hz with a sampling frequency of 0.0011 Hz.

Precipitation

The precipitation data collected at Marsh Landing is reported as total daily precipitation. Since the CTD sondes recorded data every 15 minutes, the water level signal remaining after tidal influences were removed, was averaged using a linear interpolation from 15 minute time points to daily values. Next, the cross correlation between precipitation and changes in tidally removed water levels was quantified, to see the response of the water level to precipitation events. Precipitation was summed over a number of days in the past. A range from 1 to 21 days in the past was used to calculate cumulative precipitation. For the correlation analysis, only data for which precipitation occurred in the time window preceding the water level measurements were used for the comparison as to not skew the data by giving a correlation with the days of no precipitation. The correlations were computed for any lags in the change in water table, which can be anywhere from 0, meaning instantaneous impact, to more than a week, demonstrating a long delay in the response of water levels to a precipitation event.

CHAPTER 3

RESULTS

Hydrodynamic Results

Salinities recorded across the transect range from a minimum of 10.4 to a maximum of 56.8 across the wells (Figure 4). The minimum and maximum occur in wells 5 and 3 respectively. Year round, the well in the back marsh (well 3) also has the most stable salinities. Temperatures across the transect had a minimum occurring at well 8 with 12.1°C and the maximum being 29.7°C at well 3. The water levels can be seen in Figure 5, after temperature, pressure, and salinity has been converted into density using UNESCO equations and water height has been referenced to the NAVD88 datum. The largest amplitudes are seen in well 8. This well also shows a resting saturated state when not inundated. Well 1, the well closest to the barrier island, has an elevated water table compared to the other wells. During the time period the wells were monitored, four different drainage events can be identified. These events were identified as water levels dropping below the saturated marsh surface and continuing to decrease for several days.

Reference Depth

The difference of pressure between well 7 and well 8 showed a potential discrepancy with regard to pressure referenced to the same elevation. For locations across the marsh in which inundation occurs, the peak water level height should be the same. Figure 6 shows that there is a small difference in peak pressure between the two

wells of 869.08 Pa. The R^2 correlation between the paired peaks was 0.9971. Once it was determined there was a consistent offset between the two wells, a correction of 869.08 Pa was made for well 7.

Slug Tests

The measured pressure from the slug test shows the same pattern for all 4 wells in which the slug tests were performed (Figure 7). The spike in pressure happens when the slug of water was instantaneously added to the well. Immediately following that step, a drop in pressure is observed until natural conditions are reached. A logarithmic curve was fit to the measured pressure after the slug was added (Figure 8) in order to get the values found in Table 3. The highest permeability was found to be $7.0*10^{-12}$ m^2 at well 1 corresponding to hydraulic conductivity of $7.1*10^{-5}$ m/s. The lowest permeability was located at well 3 with $2.3*10^{-12}$ m^2, corresponding to hydraulic conductivity of $2.32*10^{-5}$ m/s.

Magnitude And Direction Of Groundwater Flow

The average velocities (Equation 3) from August 2011 to June 2012, between all the wells, were positive (pointing from Blackbeard Island towards the marsh) except the average velocity between wells 3 and 4, which was negative (from the tidal creek towards the barrier island) (Table 2). Figure 9 shows the Darcy velocity patterns across the transect, with the saturated marsh (between wells 7 and 8) exhibiting near constant creek-ward flow when not inundated. Tidal patterns can be seen influencing every well. The largest amplitudes are seen between wells 5 and 7. The averages of these velocities represent the water table gradient across the marsh as the tidal forcing gets averaged out and the overall gradient remains.

Subsurface Pressure Waves

Figure 3 shows the impact of the propagation of the tidal signal through the subsurface using equation 15. In this scenario a hydraulic conductivity of $2.3*10^{-5}$ m/s, which is representative of the marsh subsurface, was used. The distance of propagation was determined when the amplitude drops below 1% of the tidal amplitude. The influence of propagation with a tidal amplitude of 0.75 m extends 22 m from the tidal creek into the marsh falling short of well 8 which is 100 meters from the tidal creek. Using the same tidal amplitude but with a hydraulic conductivity of $7.0*10^{-5}$ m/s, which his representative of the upland, the influence of the pressure wave is nearly doubled to a total reach of 39 meters.

Density Driven Flow

There are two main factors that directly affect the pressure gradient: changes in fluid density and changes in piezometric head. Equations 12 and 13 define two separate pressure gradients between each well pairings, one due to density variations (Equation 13), the other due to head changes (Equation 12). The impact of density variations across this transect can promote flow either towards the tidal creek or toward the barrier island (Figure 11). The relative impact of density driven flow compared to piezometric head can be as large as 16% as seen in the gradient between wells 3 and 4 (Table 4), however the flow between these wells have the lowest overall velocity (Table 2). The smallest impact of density driven flow across the time series was seen between wells 2 and 3 with a maximum of 3%.

Tidal Frequency Analysis

When the water level time series of well 8, the most creek-ward well, was analyzed using U_Tide, 55 of the possible 59 tidal constituents identified were statistically significant (Table 5). The constituent that had the largest impact was the M_2 tide with an amplitude of 0.111 m and a percent energy of 34.4%. When the reconstruction of the pressure signal created with U_Tide was removed from the original signal, values as high as 0.6 Pa and as low as -0.4 Pa were observed (Figure 12).

When looking at the water level signal of well 8, a value of 0.4668 m was chosen as a cutoff, to remove the portion of the signal that is non-sinusoidal. This was chosen due to all points above this value had clear tidal patterns and the saturated values were removed. As the time series showed a near constant water level when the marsh was not inundated but remained saturated, all data below a cutoff was omitted from the signal. To be able to conduct the analysis on an irregular signal, U_Tide scales the covariance using Lomb-Scargle periodogram instead of a Fourier Transform (Codiga 2011). When the exact same steps were applied, the number of statistically significant constituents dropped to 52 (Table 6). The largest constituent was still the M_2 tide. Although the amplitude of this constituent increased to 0.130 m, the percent energy of the constituent dropped drastically to 13.42%. The reconstructed tidal signal from U_Tide shows that the artificial signal now extends below the saturated elevation (Figure 13).

Empirical Mode Decomposition

EMD identified 15 individual modes from the water level of well 8 (Figure 14). The highest amplitudes observed can be found in mode 5 with an amplitude of 0.8 m.

The last mode, mode 16 is the baseline, which is centered around 0.5 m. The remaining modes have an amplitude centered on 0 m. Within the first five modes, the M2 tidal constituent can be distinguished (Figure 15). As the modes change from 1 to 15, there is a decrease is the frequency of the largest amplitude per mode. Likewise, as the modes decrease, so does the number of frequencies seen per mode.

Empirical Orthogonal Functions

The EOF analysis results in 7 different functions when all 7 wells are included and implemented in the input matrix. When the eigenvalues are computed to explain variance for each function the results starting at the 1st function to the 7th function are: 70.62%, 19.04%, 7.37%, 1.55%, 0.88%, 0.43%, 0.11%. The first three functions equate to 97.03% of the water level signals. The amplitudes of the different functions are shown in Figure 16. The largest amplitudes are seen in the first function and continue to decrease to the smallest amplitudes seen in the last function, function 7. Semi-diurnal tidal patterns can visually be seen in all 7 functions but become most prominent in functions 2 through 7. A scalar value is associated with each function and location (Figure 17). This scalar can be either positive or negative and range between 1 and -1. Across the wells, functions 2 through 7 have both positive and negative influences. The only function in which the sign remains constant is function 1 with a negative influence on every well. Function 2 has both positive and negative values, with a pattern that follows marsh elevation such that wells 1 and 5 show a positive impact from this function. The largest scalar is seen at well 1 with the following two values occurring at wells 2 and 5. The lowest elevation is seen at well 8 and has the largest negative scalar.

Inundation Meter

After the threshold was used to determine tidal inundation at well 8, 718 different occurrences of inundation were identified during the August 2011 to June 2012 time period (Figure 18). During this time period around 600 occurrences of tidal inundation should have been identified. The extra occurrences identified are occurring due to small pressure fluctuations while the marsh is not inundated. After the threshold was used to remove tidal inundation from all the wells, a clear tidal influence still remained (Figure 18b). To remove the remaining tidal influences, three approaches were implemented. In Figure 19, the result of the first method, using the threshold twice is in the light blue dots. The second method in dark blue dots is from when a low pass filter was applied to the inundation-removed signal. The final method used was identifying the low peaks, resulting in a signal shown by the green dots in figure 19.

Precipitation Analysis

The cross correlation analysis between the change in water level and the accumulation of precipitation (Figure 20) produces several hundred correlations, one for each of the three approaches used to removed tidal impact, for each lag studied, for each duration of cumulative precipitation considered and for each well. To condense these results, only lags that are positive are considered, i.e. correlations between precipitation and changes of water levels in past are ignored. Within the remaining values, the highest 10% of correlations between water level and precipitation for each of the wells and the three methods. Averages and standard deviations of these r-values, and the associated lags and time windows over which cumulative precipitation were computed to quantify the magnitude and the variability in lags and precipitation leading

to similar correlations (Table 7). The highest correlations are seen using the low pass filter method compared to the other two methods, which gives a range from an r value of 0.662 for well 1 to an r value of 0.243 in well 8. Each method has well 1 with the highest correlation and well 8 with the lowest. Across the three methods, the shortest lag time was seen at well 1. The highest lag was observed within the first method at well 8, having a value of 50 days. The lowest lag was seen in the second method at well 2 having a 0.5 day lag.

CHAPTER 4

DISCUSSION

Flow Patterns

An important step for comparing flow patterns within the marsh is referencing all the data to the same NAVD88 reference depth. This step allows for correcting pressure that simply reflects gravitational forces, which does not affect horizontal flows. The average depth of all the sensors was chosen to be the reference depth to limit errors. By using the average depth, it minimizes the total depth change between the sensor depths and the reference depths. Minimizing these distances reduces the chances of salinity and temperature changes.

Another correction was applied to the data obtained in well 7. The error identified in the elevation data would have affected Darcy velocities at that location substantially, as a small offset in elevation can have a profound impact on pressure gradients. The error in the raw measurement may be due to an error in recording the piezometer dimensions. If any one of the measurements from Table 1 is incorrect, the offset in the data will be consistent through the entire time series. The outliers from the relationship seen in figure 6, all occur during the lowest high tides, where pressure is lowest, allowing additional influences to be present.

Across the entire transect a variety of marsh environments is encountered. Wells 1 and 5 represent two different types of upland settings, mainland and a hammock respectively. The transitional environments are represented in wells 2 and 4. The

remaining wells represent the marsh platform which extends across the majority of the transect. Before any of the flow patterns across the marsh can be determined, an accurate understanding of the sediment porosity and hydraulic conductivity must be investigated. Four locations were chosen to conduct the slug tests; wells 1,3, 5, and 8. With the upland wells having the highest permeability, groundwater has the potential to flow through these environments at a higher velocity. However, the aquifer permeabilities only vary slightly (about a factor of 3) across the transect. As the groundwater flows from the upland (Blackbeard Island) to the hammock, not only does the permeability change but so does the flow gradient (figure 9, see below). This gives the flow coming from Blackbeard Island consistently some of the highest flow rates (Table 2). The marsh platform is saturated year round due the muddy composition of the marsh in correlation with the marsh being regularly inundated.

Impact of Salinity Distribution

Across the domain, one of the most dynamic measurements taken, next to pressure, was salinity (Figure 4). Salinity is one of the main factors in determining vegetation distribution across a salt marsh (Bertness and Ellison 1987). Despite the relatively small length of the transect of just over 200 meters, there is an average difference of 42.4 g/kg between the most saline well (well 3) and the freshest well (well 5). With the lowest salinity occurring at the hammock (well 5), there is a potential for large gradients occurring off the hammock as shown in Figure 11. The direction of density driven flow will be both ways being towards and away from Blackbeard Island. The large gradients in salinity in such a short distance will cause vegetation zonation to form due to competition (Pennings et al. 2005). At well 8, the creek-ward most well,

Spartina alterniflora is found. As you move towards the hammock at well 7, *Juncus romerianus* is found. The transition between well 7 and the hammock is where the *Borrichea frutescens* zone is. As you get behind the hammock into the back marsh, the highest salinities are seen. Spartina is the plant that has the best ability to survive in these kind of environments (Bertness 1991).

Influence of Pressure Wave from Creek

Schultz and Ruppel (2002) measured the response of the groundwater table due to tidal forcing and determined that the upland hydraulic conductivities to be 10^{-4} m/s in the clean sand of the upland, which is supported by the permeabilities reported in Wilson (Wilson et al. 2008) of coastal marine sediment. The values found from the slug test were ~10^{-5} m/s for the upland and marsh. The hydraulic conductivity determines how the tidal forcing propagates from the tidal creek within the marsh. The 1D model (Figure 10) describes the response of the groundwater table with a known hydraulic conductivity. This is a simplified representation of this marsh transect which lacks in two main aspects. First, it does not allow for variable heterogeneous sediment composition across the marsh. However, the slug tests demonstrated that throughout the transect, the hydraulic conductivity, does not vary more than an order of magnitude so can be accounted for by one value. Second, the model does not account for the inundation of the marsh platform from the tidal creek, as in Schultz and Ruppel (2002) the high tides alter the head gradient, but never overtops the creek bank. There is the potential that as the water inundates the marsh, the pressure associated with this additional water mass will alter the flow patterns.

In many marshes in the southeast, the tidal creek is much closer to the hammock and back marsh than at our study site and hence a subsurface pressure wave from the tidal creek would have an influence on the pressure signal at the wells. This influence will change groundwater movements across the transect as the additional force is exerted on a water parcel. The lower permeability of the marsh still greatly reduces the distance and amplitude of this influence. The sediment composition of a beach face allows tidal forcings to be measured further in the transition zone between the water and subsurface aquifer.

EMD and EOF

EMD was utilized because it decomposes a complex time series into modes without strong assumptions on the nature of and periodicity in the signal. An FFT was conducted to identify tidal components in each mode. FFT analysis (Figure 15) showed that mode 5 and 6 were dominated by the M_2 tide.

EOF was used to examine patterns in water level signals over space and time. The result is 7 different functions that can be used to explain the system as a whole. Similar to the modes from EMD, it is difficult to discern the meaning of each mode. The first three functions explain a majority of the variance within the transect. The first EOF has the highest variation in amplitude (note scale in top panel of Figure 16), and the mode has the same (negative) sign at all locations, so that it impacts all wells similarly. The amplitude of the first EOF time series shows patterns that are similar to those seen in the water table when it drops below saturation. As it is similar across the transect, it is interpreted to reflect larger scale water level. The second EOF function shows amplitudes that resemble tidal forcing (Figure 17). Notably, the pattern in the second

mode resembles the topography, and its impact changes across the transect, indicating a positive influence in the upland and hammock and a negative influence on the marsh.

Tidally Driven Flow

Oceanographers have a powerful tool, U_Tide, to identify the signal contribution at tidal frequencies from any time series. When working with water level time series in the ocean or in a bay, this tool can work to great accuracy (Codiga 2011). Adapting this tool to do the same thing for a groundwater signal in a saturated marsh proved more difficult than first anticipated. When first run on the raw water level signal, the reconstructed signal using tidal frequencies only has an amplitude near the same value as the raw data. However, because the original and reconstructed signals don't line up, the residual signal has an amplitude comparable to the raw signal (Figure 12). Since majority of the well 8 water level signal is driven by tidal inundation, it was determined that a comparable amplitude meant a failure in the method. This problem stems from one major flaw when applying U_Tide to the well water level signal. The raw water level signals for the salt marshes were fully saturated for majority of the year. This does not allow for individual frequencies to have a complete sinusoidal signal. The frequency fitting that U_Tide is capable of does not include non-sinusoidal signals.

U_Tide has a built in ability to deal with data gaps. This allows water levels that reflect the saturated marsh to be removed. However, when U_Tide was applied to such a reduced data set, a similar result was seen, meaning amplitudes of the residual signal were still similar to the amplitudes of the raw signal.

The saturated marsh may cause using U_Tide to fail but it allows for a more direct approach to be taken to remove the tidal influences. The creek-ward most well

(well 8) is one of the locations in which the subsurface is fully saturated for most of the year. One assumption must be made that all water levels that are above the marsh platform are directly from tidal inundation. Well 8, can be used as an inundation meter, identifying the timing when the incoming tide overtops that location. The tidal inundation impacts the entire domain by either inundating the marsh or influencing the pressure from the surrounding area. The only wells, which do not get inundated during the time period of the study, are wells 1 and wells 5. Removing direct inundation allows for additional patterns to be seen, and be correlated with other forcings, such as precipitation (Figure 18).

The most noticeable pattern once direct inundation was removed was the remaining influence of tidal patterns. These remaining tidal frequencies in the signal are thought to be due to subsurface pressure waves being exerted as the tide rises and falls. The subsurface pressure wave from the tidal creek was previously negated as an influence upon the transect. As a flooding tide inundates the marsh, the force exerted by the added water mass exerts a force on the subsurface in the surrounding area. The pressure directly associated with the over topping inundation was removed however this additional force remains. The three different attempts to remove this remaining tidal signal (Figure 19) approach the problem in similar ways. The base flow in this problem will contain the remaining drivers of flow while removing the influences due to tide.

Precipitation Across the Marsh

Once the majority of the drivers removed or found to be of minor importance (subsurface pressure wave from tidal creek, density driven flow, direct tidal inundation, subsurface pressure waves from inundation), precipitation can be compared to the

remaining signal. As precipitation events occur across the domain, there will typically be an equal blanketing of rainfall occurring throughout the transect. However the upland most well (well 1) has more favorable conditions to see the effects of precipitation. Consistently across the three different methods implemented, well 1 had the strongest correlation with precipitation (Table 7). This favorable condition may largely be due being located at the transition from the upland to the marsh. The correlation begins to diminish further away from the upland well. The correlation found at the upland well on the hammock is not as strong for well 1. This is most likely a factor of the size of the hammock vs. the upland barrier island. The effects of a precipitation event would be less seen because less water can be collected from the hammock surface. The larger barrier island (Blackbeard Island) allows for the upland to gather the precipitation where the effects can be felt the most at the transition from the upland to the marsh.

The second part of the precipitation analysis involved looking at the accumulation of precipitation between 1 and 21 days prior to the precipitation event. The three methods varied greatly with this result. No discernable pattern could be identified within each well. The method that gave the highest correlation coefficients also resulted in the most similar ‘days of past accumulation’ across the transect. This would suggest that the water levels in the different wells respond similarly, having the strongest correlation with the rain events occurring collectively within just over two weeks.

Dominant Forcing

Previously it was identified that the marsh platforms for this transect remain saturated for the majority of the year when not inundated. This has a major impact on how groundwater will flow throughout the marsh. Tidal patterns can be easily identified

in signals that represent the full sinusoidal nature of the tides. Precipitation has a greater chance of becoming run off rather than percolating into the subsurface. The saturated marsh not only influences the groundwater flow, but how we analyze this flow. The non-sinusoidal signal limits what type of frequency analysis can be performed. Frequency analysis on a non-sinusoidal signal is mathematically more difficult.

Of the 7 well locations across the transect, 6 wells are regularly inundated. Tidal inundation brings a large body of water at different frequencies depending upon location in the marsh. The overall pressure gradient due to the tide will have a near zero net effect on groundwater flow. A deeper understanding of how tidal inundation is influencing groundwater movement can be gained by considering the moving average of the water level gradients for all the wells with varying time windows. Four moving average windows were applied; on that encompasses the M_2 tide (12.42 hr), one extending to the the K_1 tide (23.93 hr), one that extends to 4 times the M_2 tide (49.68 hr), and on spanning the M_f tide (327.67 hr). When the moving averages are applied to the water level gradients, the tidally-driven increasing and decreasing gradients are averaged out of the signal. The difference between the raw water level gradient and the averaged water level gradient will give the influence of tide within that frequency range. This tidal influence was then converted into a Darcy velocity using Equation 3.

To estimate the distance a water parcel in the subsurface moves over a flooding tide, the computed Darcy velocities were multiplied by a duration of flooding and ebbing, respectively. To convert Darcy velocities into a distance a water parcel travels during one semi-diurnal tidal cycle, the equations are:

$$L = \frac{sum(v(v<0))}{t_{total}/M2} * \Delta t \qquad (16)$$

$$L = \frac{sum(v(v>0))}{t_{total}/M2} * \Delta t \quad (17)$$

where L is distance in m, v is the Darcy velocity in m/s, Δt is time step in s, t_{total} is the total time of the time series in s, and M_2 is the period of the M_2 tide. The result of these two equations are the distance a rising and falling tide can move water in the subsurface at the depth of the sensors (Table 8). All the differences between positive distance traveled and the negative distance traveled are positive, except between wells 3 and 4. This implies that the water table for the transect flows towards the tidal creek. When the various frequencies are time averaged on the water level gradient, distances between $4*10^{-3}$ m and $4*10^{-4}$ m are seen. Thus, as the tide floods the marsh during each tidal cycle, that forcing is moving the water back a forth by only a few millimeters. As the tide begins to ebb, the water parcel is then brought back towards the original location but due to the elevated freshwater head on the island, has moved slightly towards the tidal creek.

The overall water level gradient is influencing the water movement. The largest velocities are seen between wells 1 and 2, resulting in a net flow from the upland to the marsh of about $3.1*10^{-2}$ m per M_2 tidal cycle. If this value was to remain constant and the groundwater were to travel in a straight distance to the creek 240 m away, it would take that water parcel a total of about 11 years to reach the tidal creek. However it is known that the velocities across the marsh change as you move towards the tidal creek. The gradient between 3 and 4 changes direction, implying that a water parcel would move out of the transect. It is likely that the water parcel would follow the hydraulic gradients of the inundating water. The time it takes to travel would increase by a great amount as now the distance is increased and the velocities will be changing towards the

tidal creek. As this water parcel is traveling towards the tidal creek it is being influenced by the tidal inundation, being pushed back several millimeters to rebound during the ebbing tide. The tidal influence on the groundwater is largest between wells 5 and 7 as seen in table 8. As the time window of the averaging increases, to capture more of the tidal signal, a greater influence due to tides is seen. The more tidal frequencies that are captured within this window will result in a greater tidal influence of a water parcel.

Density plays an important role on the ecology of the domain. Even with the large gradients seen across the marsh, the percent of impact remains small. Density's role in driving groundwater flow may not be a large factor in a salt marsh because of a low hydraulic conductivity (Martin 1996). The largest percent impact due to density occurs where the Darcy velocities are the lowest (Figure 21). The influence of tide and the water table will control flow, while distributing salinity throughout the marsh.

Unlike tidal inundation, precipitation does not have a rapid influence on groundwater movement. The impact of precipitation occurs over a longer time period. That time period can be over two weeks in the upland to 2 days in the marsh near the tidal creek. The largest correlation to precipitation occurs in the upland wells. The water table is recharged through precipitation. Overall the correlations between the water level signal with tide removed and precipitation events aren't significant. It is likely that the signal has additional forcings controlling flow rather than being dominated by precipitation.

There are two main possibilities for the remaining influences on groundwater flow across the domain. The first possibility could be solved by using ground-penetrating radar to look at the subsurface composition. While the observational data showed a

consistent confining unit below the sondes, aquifer leakage from a deeper, higher pressure, aquifer would add an additional force on the system. Each vibracore taken adjacent to the wells had a confining clay layer. However the depth beneath the surface and the extent of this layer varies. A pinching off of one of these confining layers could lead to aquifer leakage. Without a confining layer across the marsh, the groundwater flow patterns could be significantly altered compared to a heterogeneous sediment composition (Xin et al. 2011). The second possibility occurs on a larger scale. Regional water table gradients could affect the overall movement of water that cannot be accounted for in this analysis. Water table measurements would need to be taken in the surrounding region to investigate this possibility. If such a gradient is seasonal or depends upon local atmospheric pressure the changes would affect the flow across our transect.

CHAPTER 5

CONCLUSION

Conclusion

Measurements of temperature, pressure, and water depths, simple 1D models, and the use of statistical tools allow the drivers of groundwater flow to be investigated. Slug tests were conducted to measure the permeability across the different transect environments. The distance from the tidal creek and the permeability of the marsh prevent subsurface pressure waves from exerting an influence on the marsh transect. Manipulating Darcy's Law allows for a pressure gradient and a density gradient to be identified. The relative impact of the density gradient was seen to have up to a 10% impact on over all flow, however that impact occurs where flow is the slowest.

The marsh is fully saturated when not inundated by the tides. This makes water level signals non-sinusoidal during these time periods. The non-sinusoidal nature of the marsh prevents different tools from delineating the tide. The reconstructed tide produced by U_Tide does not successfully remove the tidal influence from the water level signal. EOF produces three functions that explain 97% variance in the signal however it is difficult to identify what controls these functions.

The saturated nature of the marsh allows the well closest to the tidal creek to be used as an inundation meter. As the tide inundates the marsh, the water level changes at this location are due to only tidal inundation. The change in water level associated with tide was implemented to identify time points in which tide is over topping the well.

The influence due to tide can be removed from the remaining wells. A tidal influence was still seen after inundation had been removed from all the wells. Three different methods were used to remove the remaining impact from the tide. Each of the three methods to remove all of the tidal influence was then compared to daily precipitation rates. The largest correlations across all three methods was seen at well 1, the well closest to the barrier island.

Tidal influence was also examined by using a moving average encompassing several different time windows over water level differences between two wells. Differences between the water levels and time-averaged signal were calculated into Darcy's velocities. An average distance per tidal cycle was found using those Darcy velocities. Each tidal cycle moves a water parcel several millimeters or less. The water table for this transect would move a water parcel from the barrier island to the tidal creek in 10 years if the velocity remained constant and a direct path was taken.

FIGURES

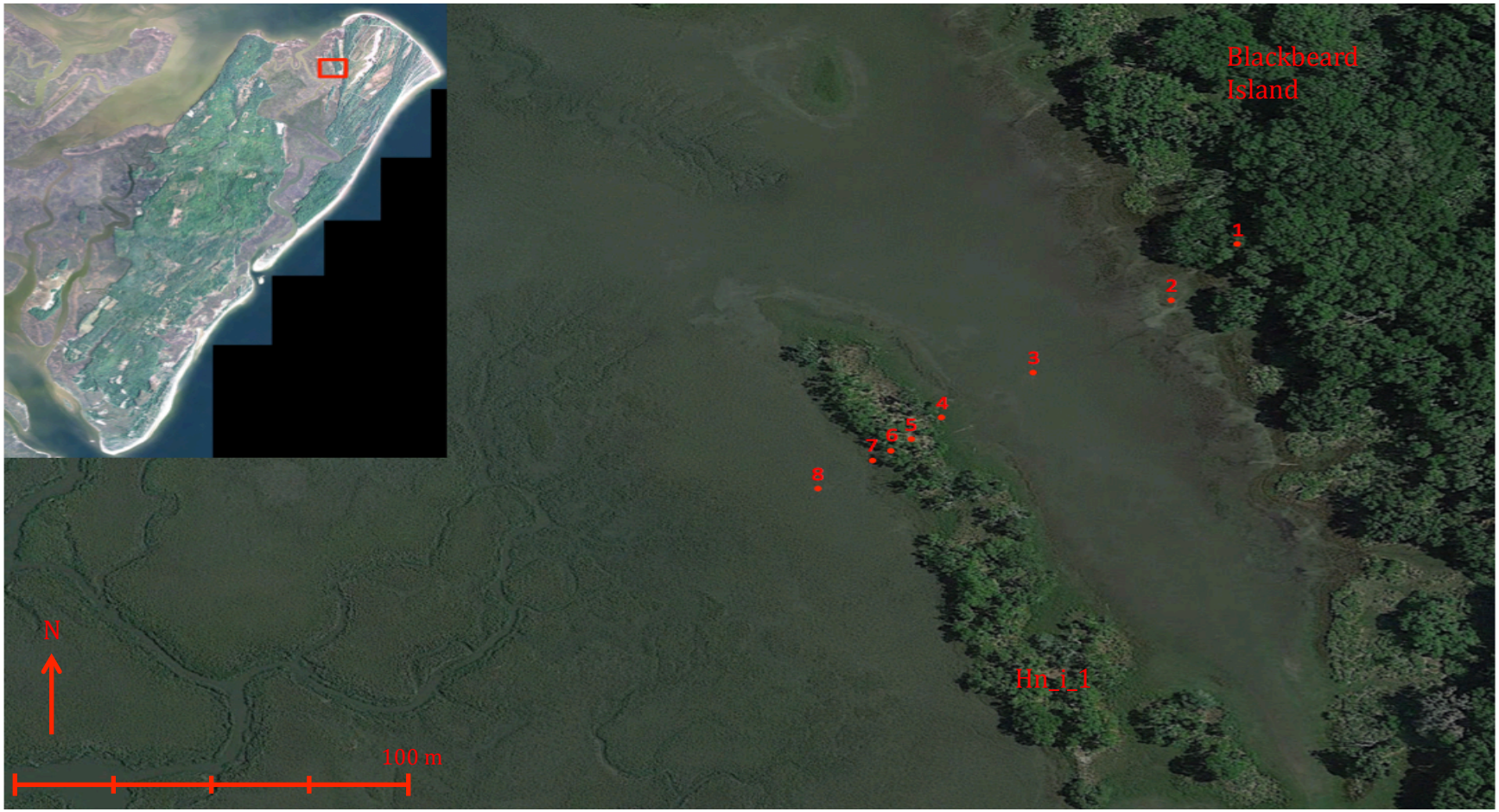

Figure 1: Study Site: The red box indicates the location of the study site at Sapelo Island, GA, at 31.51881° N and 81.20945° W. Overview of the study transect with well locations indicated by the associated well number.

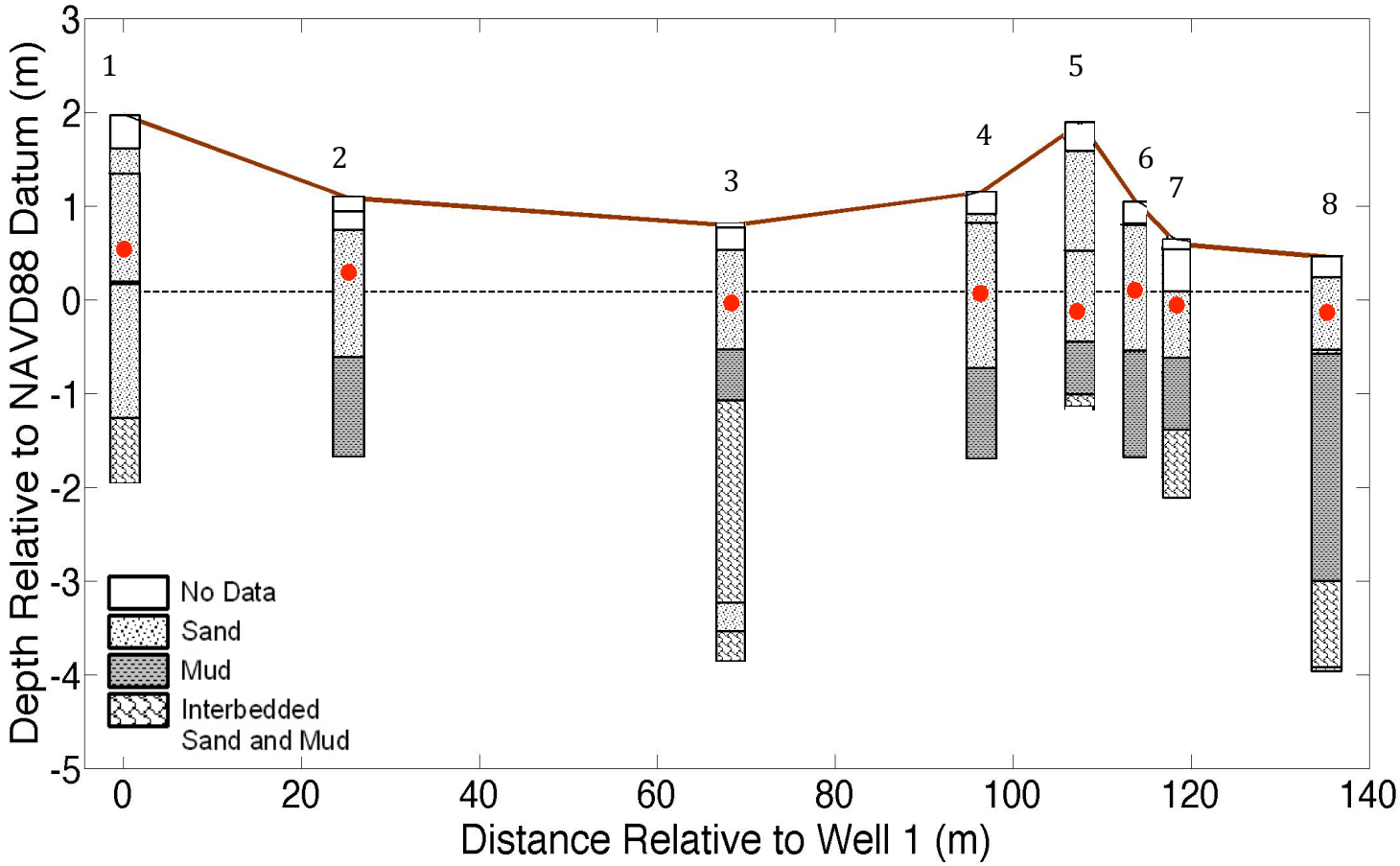

Figure 2: Cross Sectional View of Transect: Surface elevations (brown line), sensor depths (red dots) relative to NAV88 and core stratigraphy are all shown. The average sensor depth (0.085 m) is indicated by the black dashed line. Vibracore stratigraphy collected and recorded by Clark Alexander. Well numbers are indicated above piezometer location.

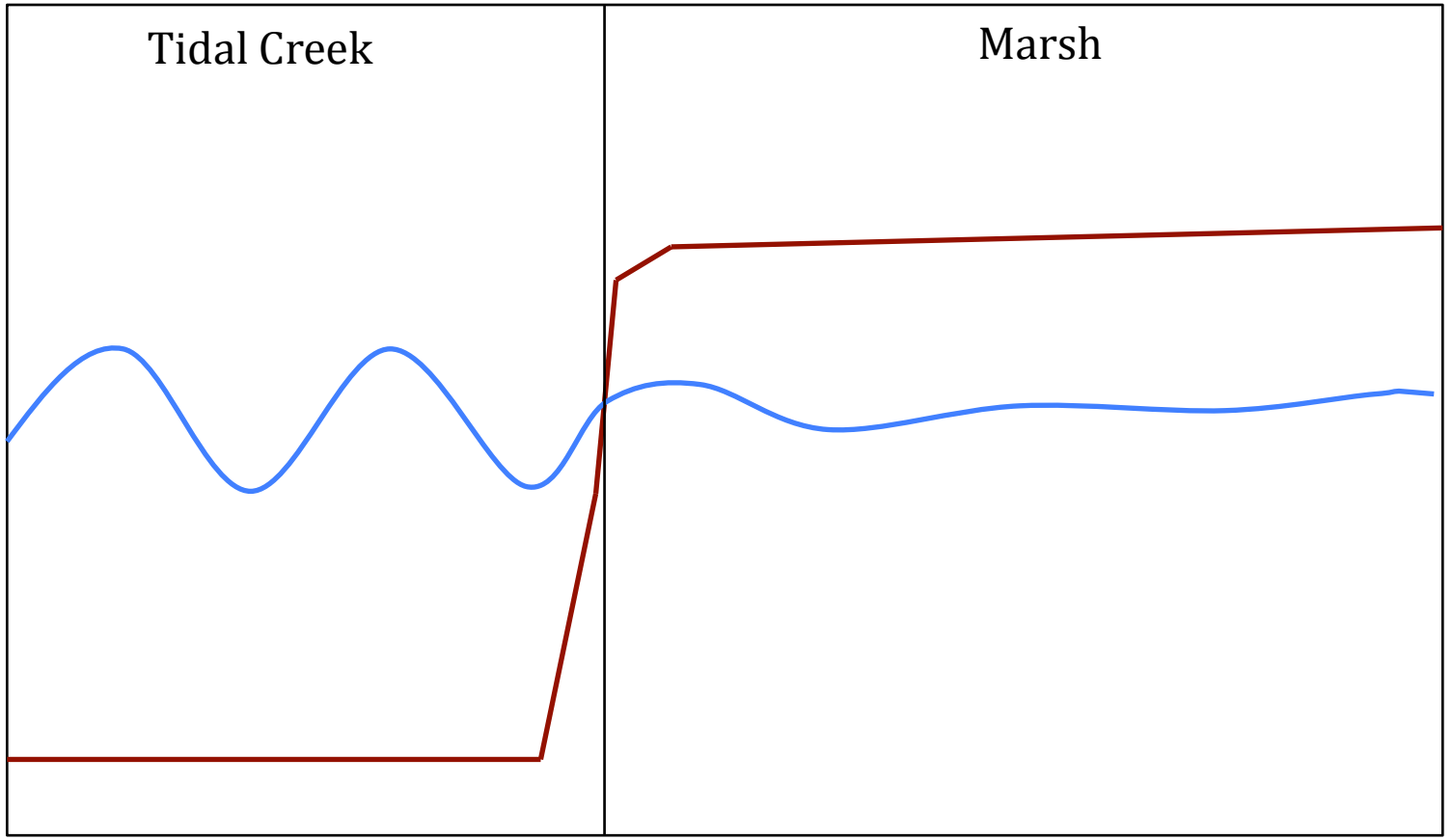

Figure 3. Pressure Wave through Subsurface: Conceptual setup demonstrating the propagation of a subsurface pressure wave from the tidal creek. Sediment surface is indicated by brown line and the blue line indicates tidal fluctuations and water table. Adapted from Schultz and Ruppel (2002).

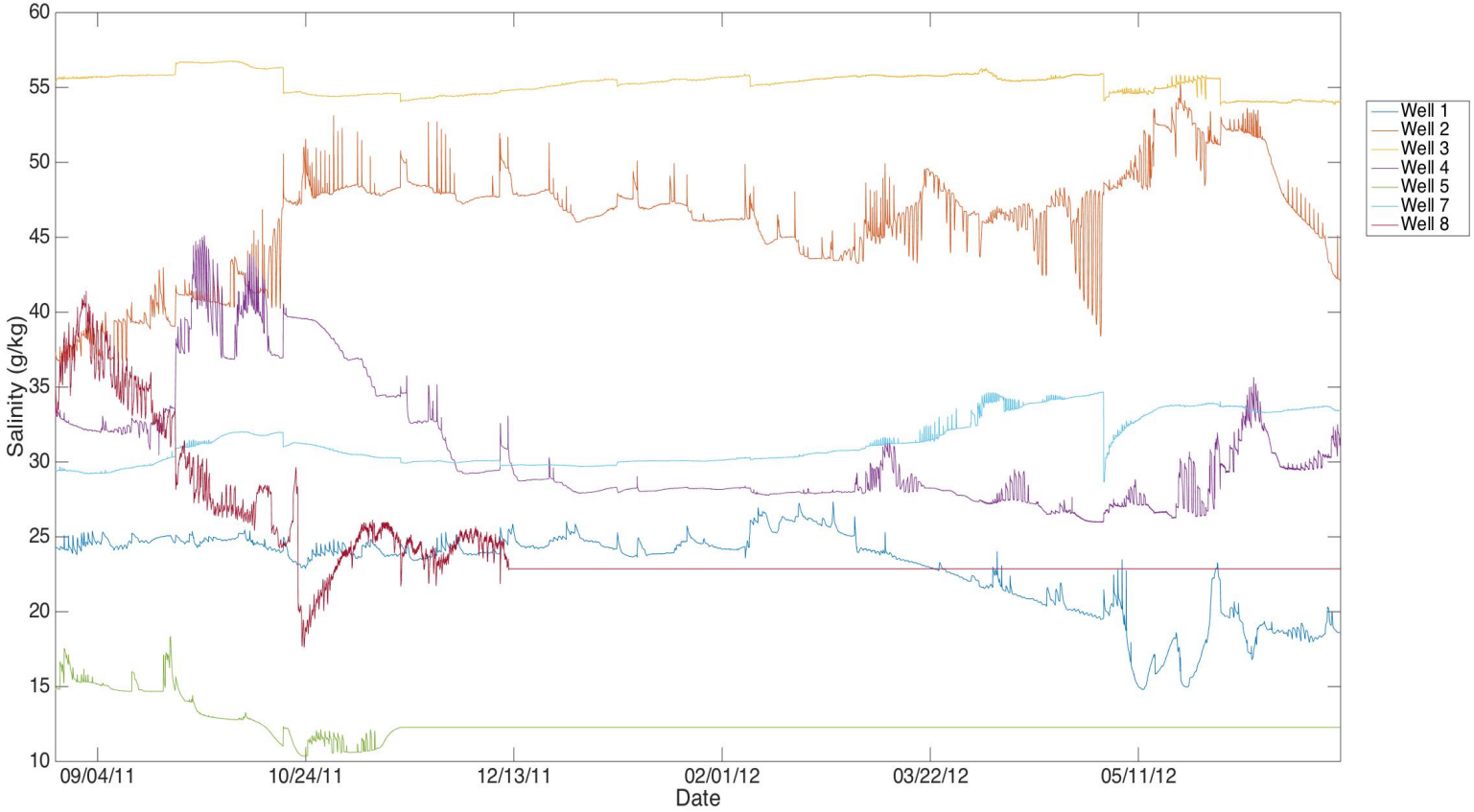

Figure 4. Salinity Across all Wells: Salinity in g/kg for all the wells between August 25th 2011 to June 27th 2012. The flat lines for wells 5 and 8 starting in early/mid December 2011 reflect failing sensors.

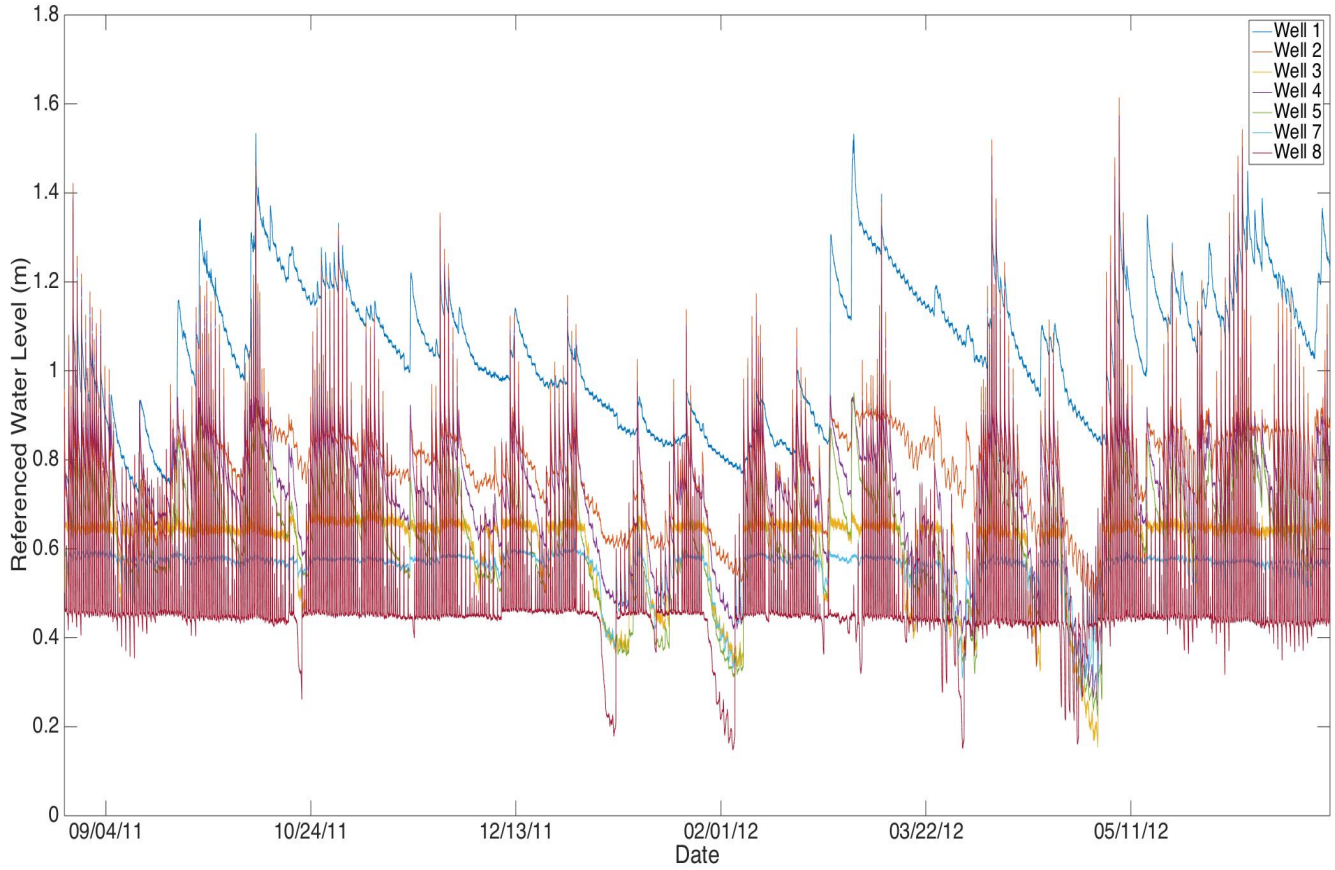

Figure 5. Well Water Levels: Water levels for all the wells across the transect referenced to NAVD88.

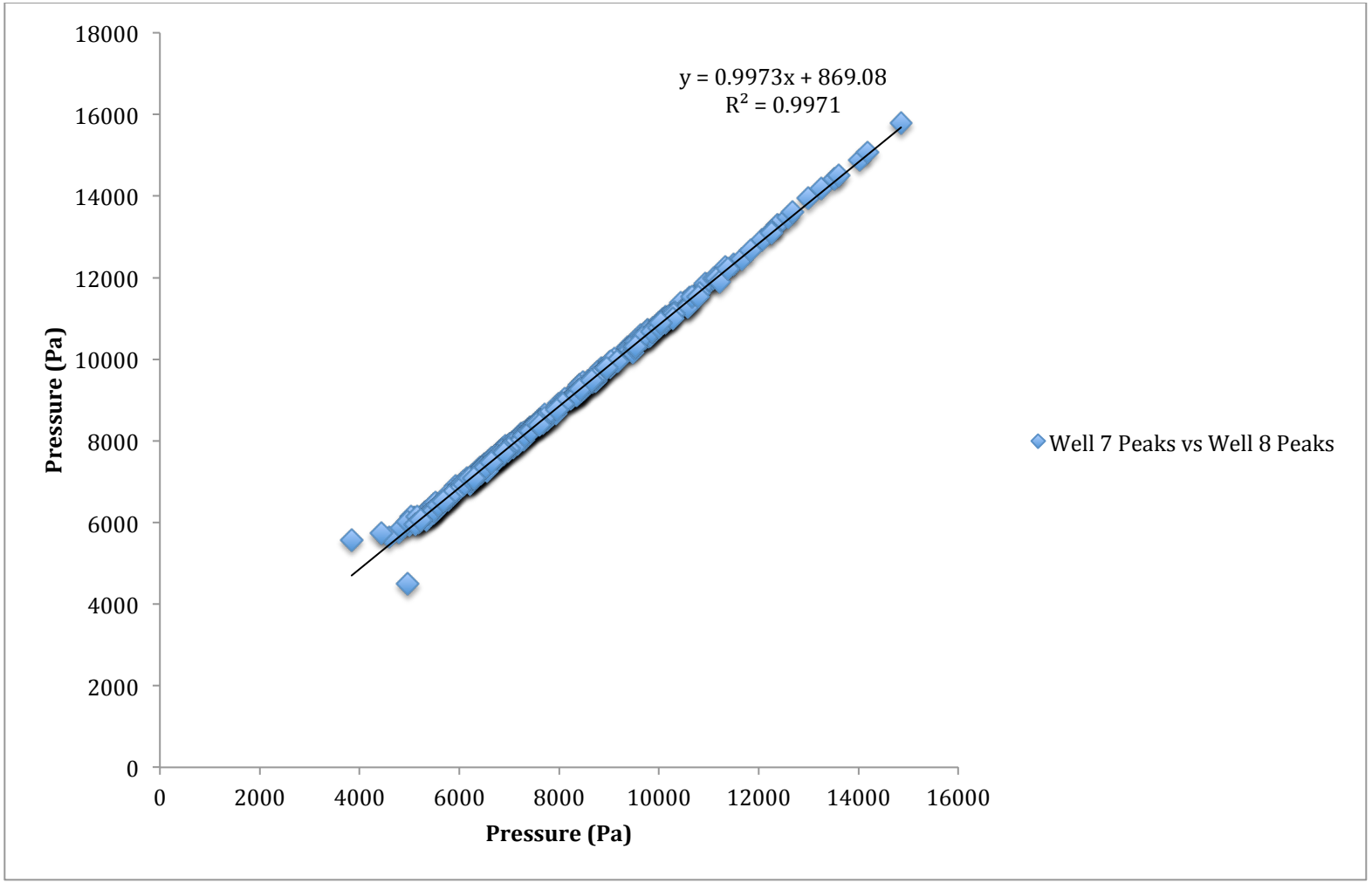

Figure 6: Peak Comparison for Wells 7 & 8: Peaks in pressure well 7 and matching peaks in pressure for well 8.

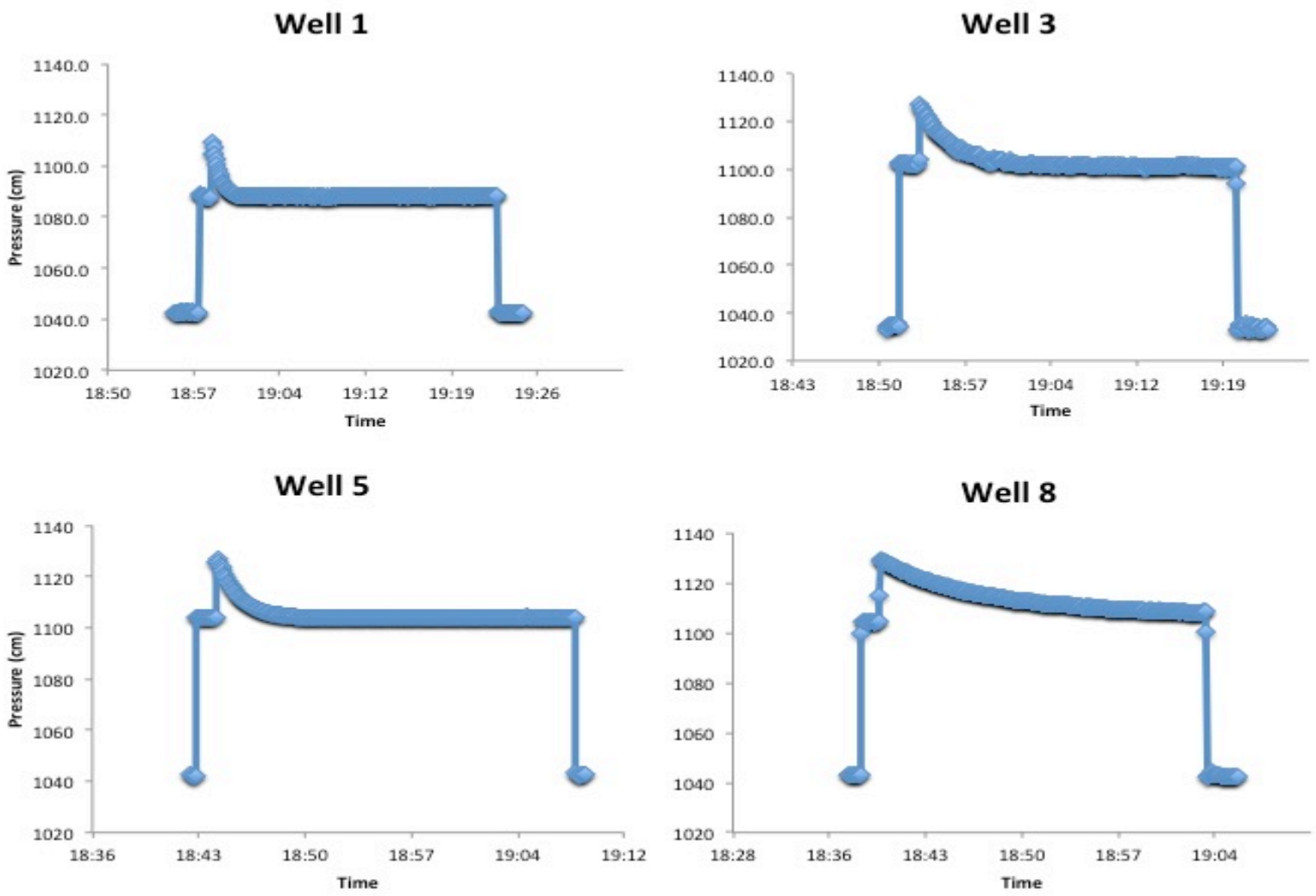

Figure 7: Raw Pressure from Slug Test: Four marsh environments were included in the slug tests; upland (well 1), back marsh (well 3), hammock (well 5), and marsh (well 8).

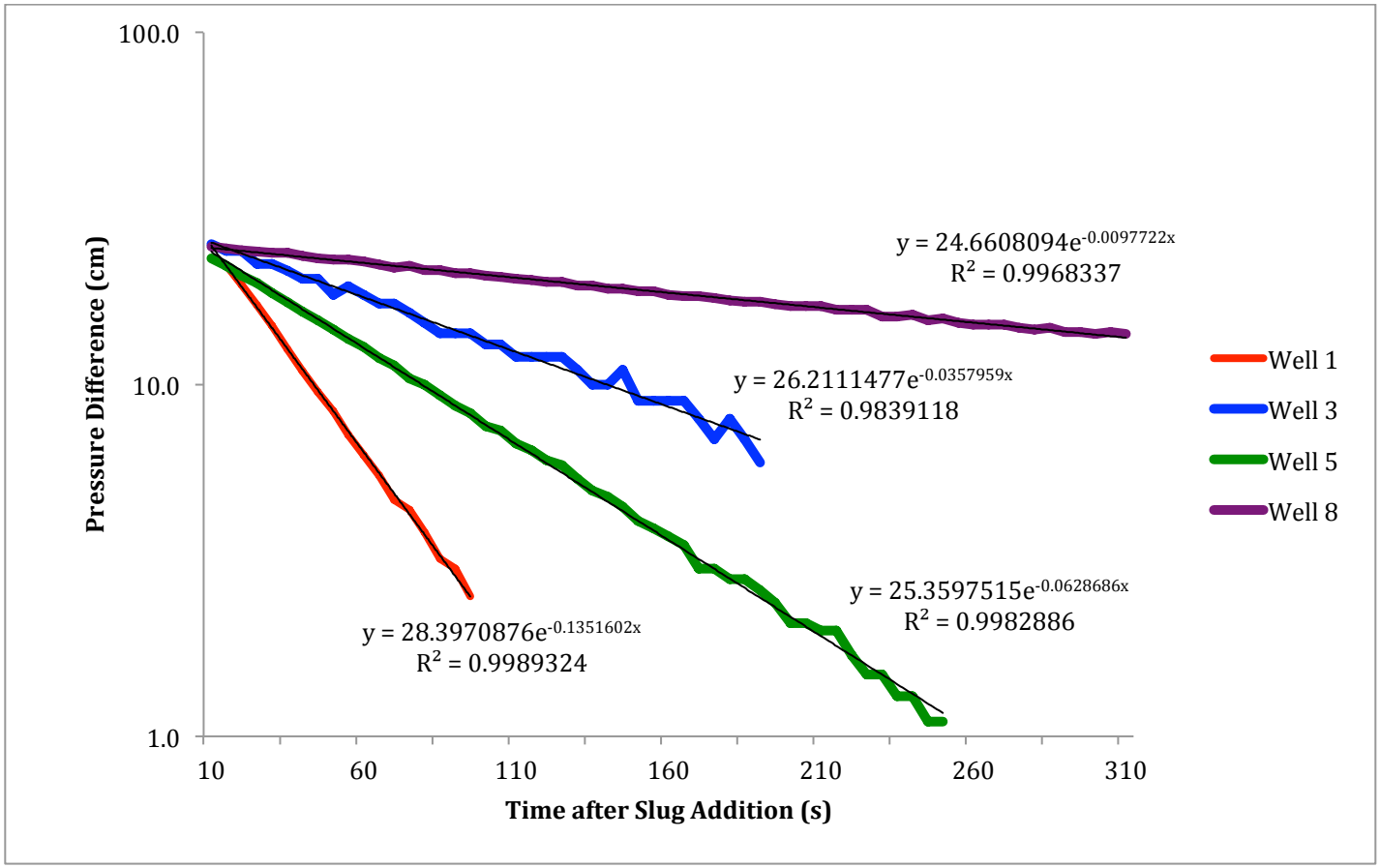

Figure 8. Exponential Pressure decay from Slug Test: Measured pressure instantaneously after slug was added on a logarithmic scale for well 1 (red), well 3 (blue), well 5 (green), and well 8 (purple). Best-fit line also plotted with subsequent equation.

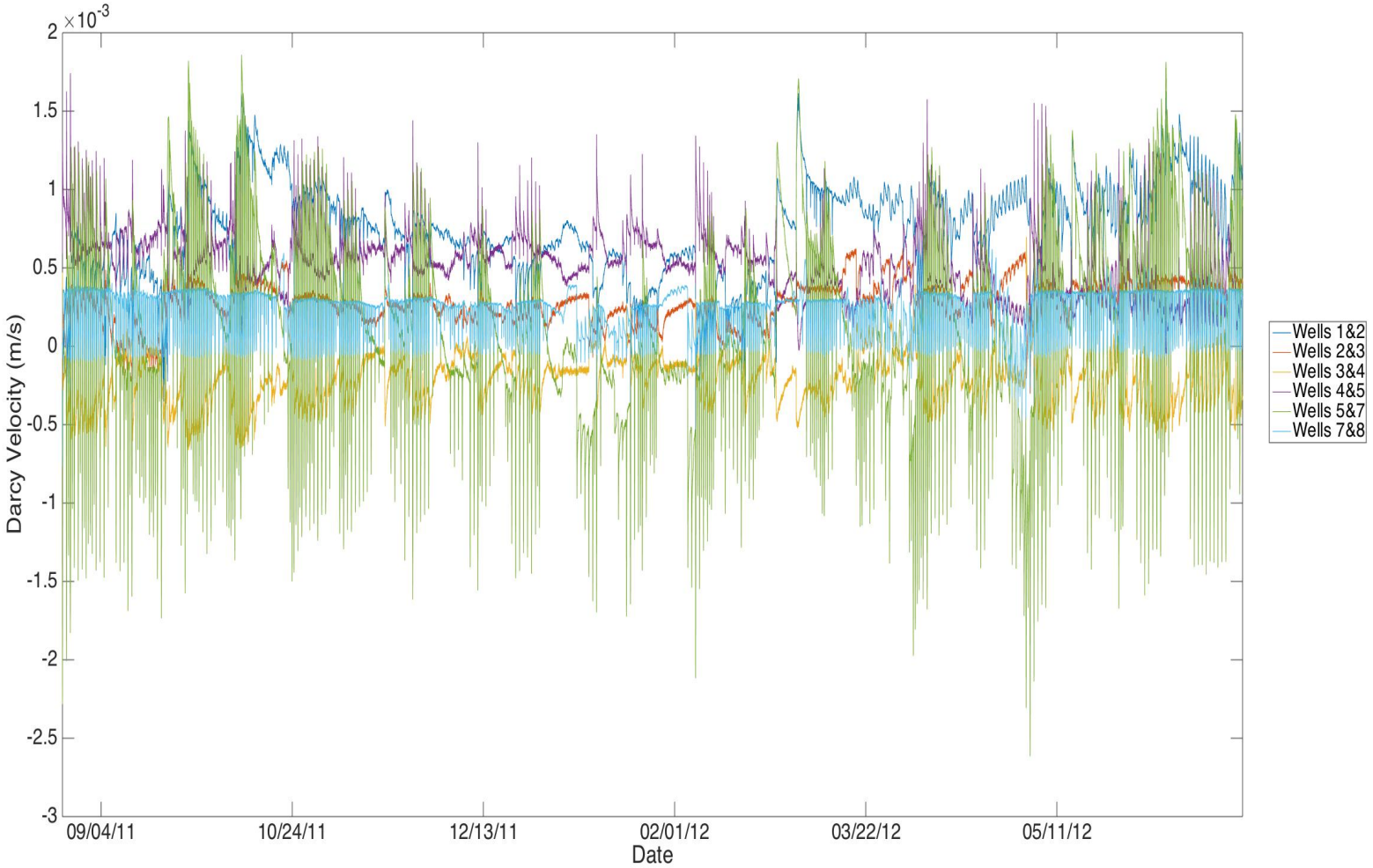

Figure 9: Darcy Velocities: Horizontal Darcy velocities between adjacent wells.

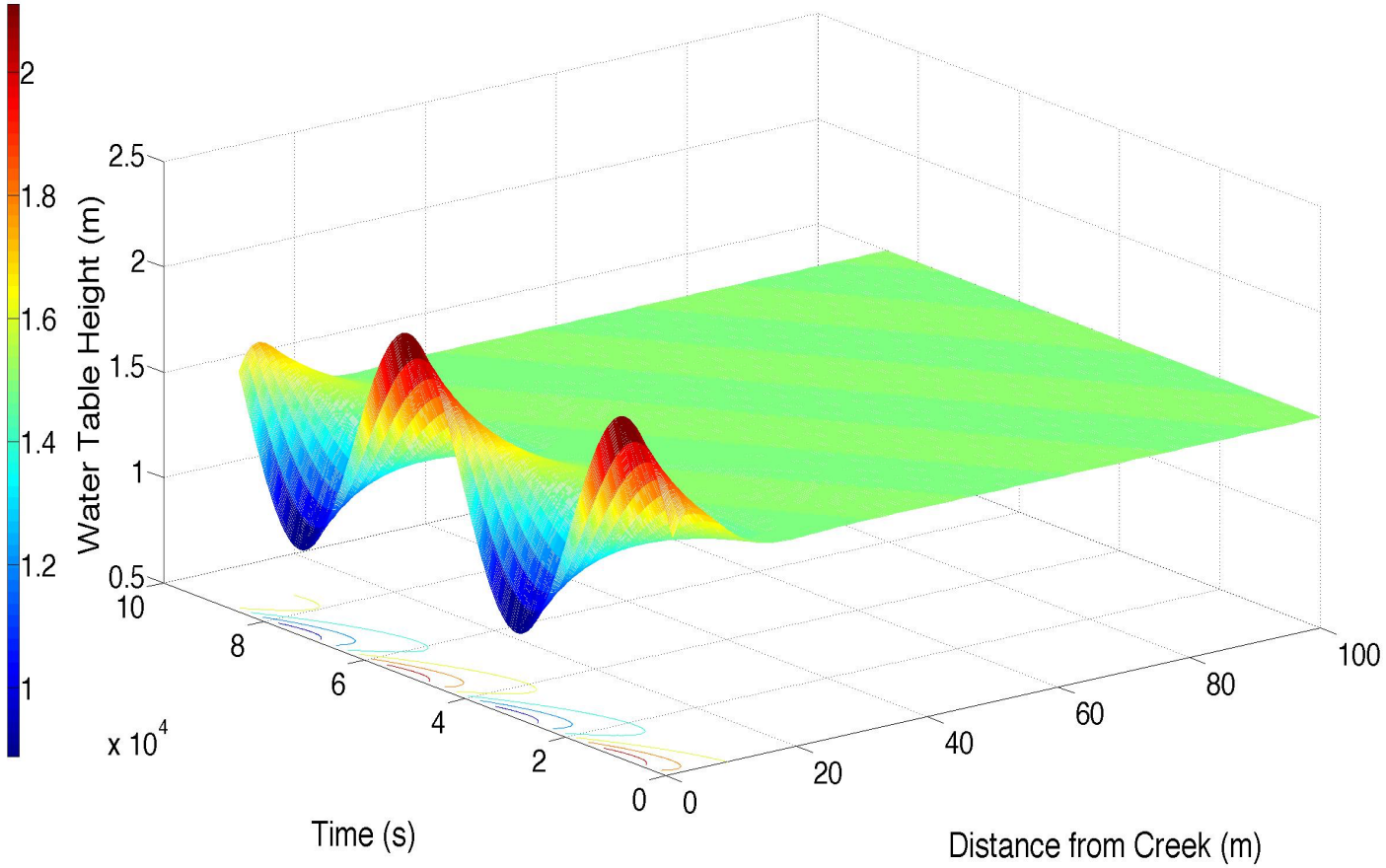

Figure 10. 1D Model of Pressure Wave: Propagation of the tidal signal through the subsurface.

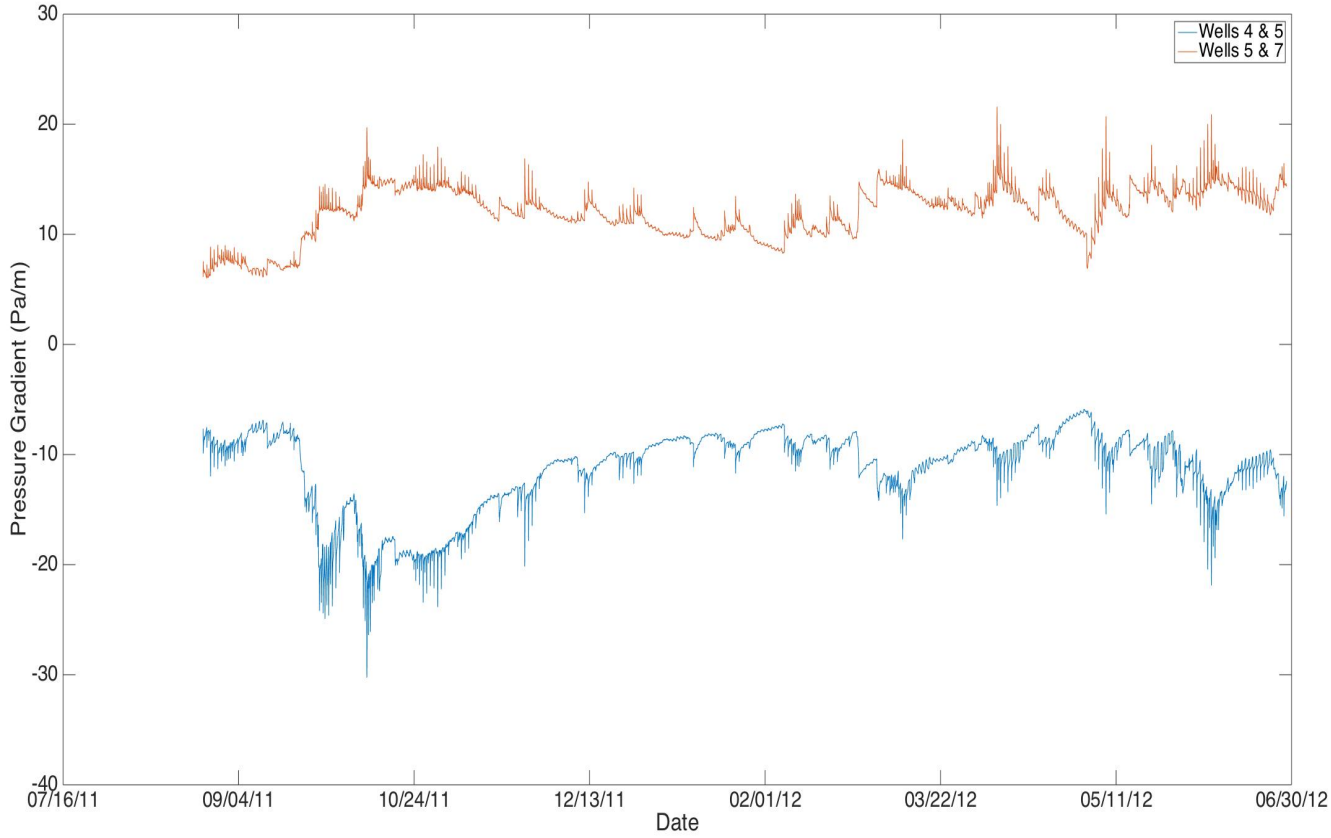

Figure 11. Pressure Gradients due to Density: Pressure gradients due to density changes for wells 4 & 5 (red) and wells 5 & 7 (black). Positive values indicate a gradient from the tidal creek towards the barrier island and negative values indicate gradients from the barrier island towards the tidal creek.

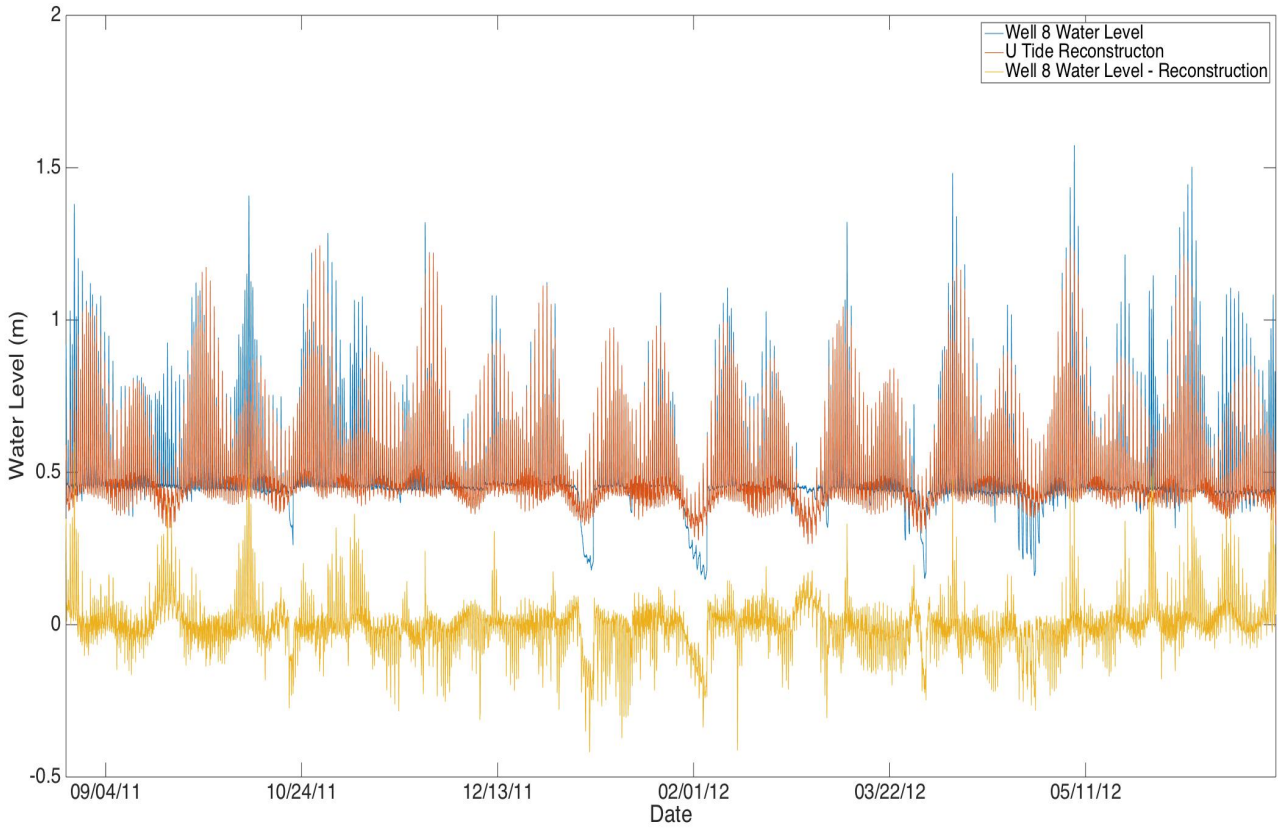

Figure 12. Projected Tidal Influence on Raw Water Level: U_Tide produced tidal projection (red) based on raw water level from well 8 (blue) and the residuals when the tidal projection is removed from the raw water level (yellow).

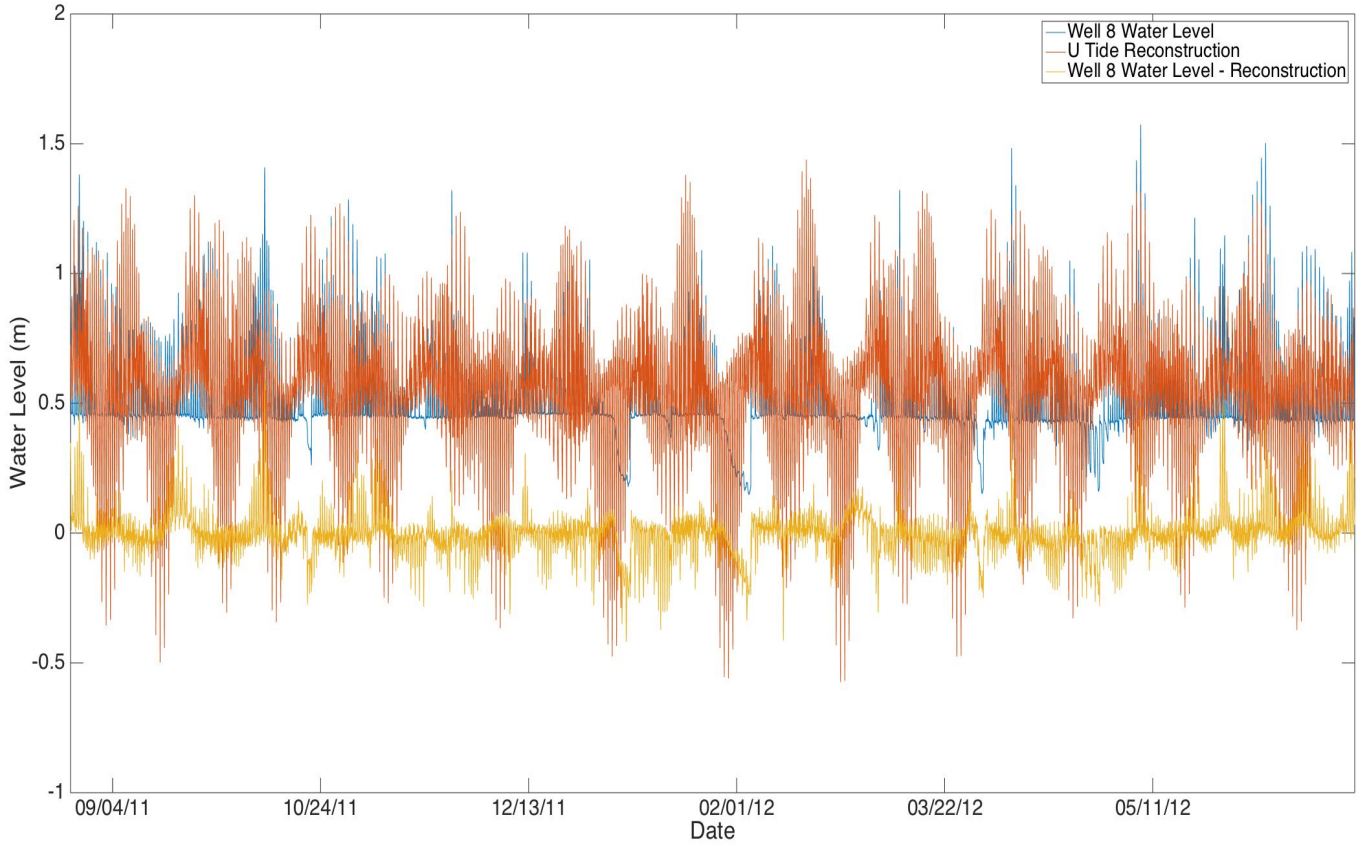

Figure 13. Projected Tidal Influence on Water Level Above Saturation: U_Tide produced tidal projection (red) based on water level values above the saturation (0.4668 m) from well 8 (blue) and the residuals when the tidal projection is removed from the raw water level (yellow).

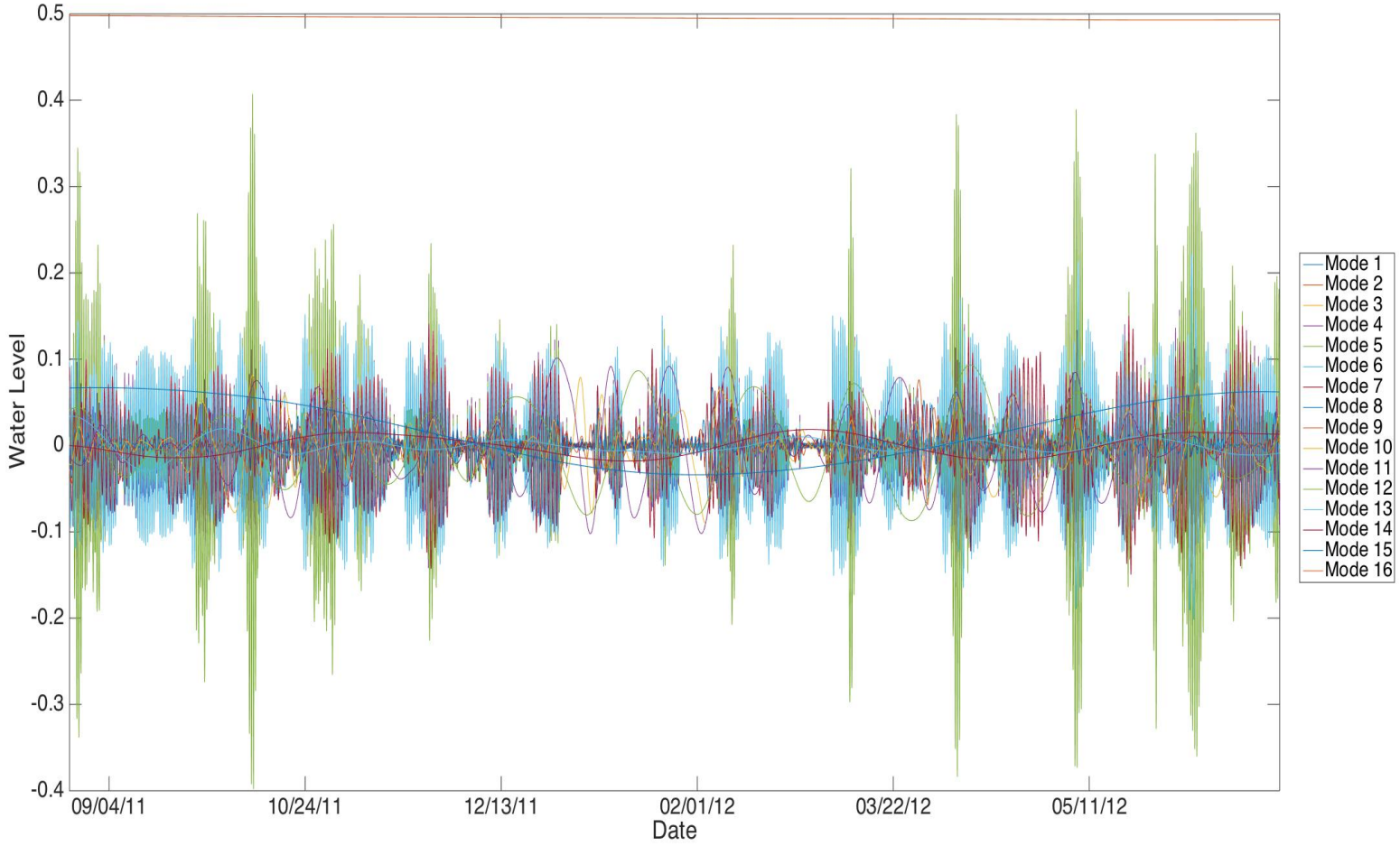

Figure 14. Modes from EMD for Well 8: Individual modes from EMD that represent well 8.

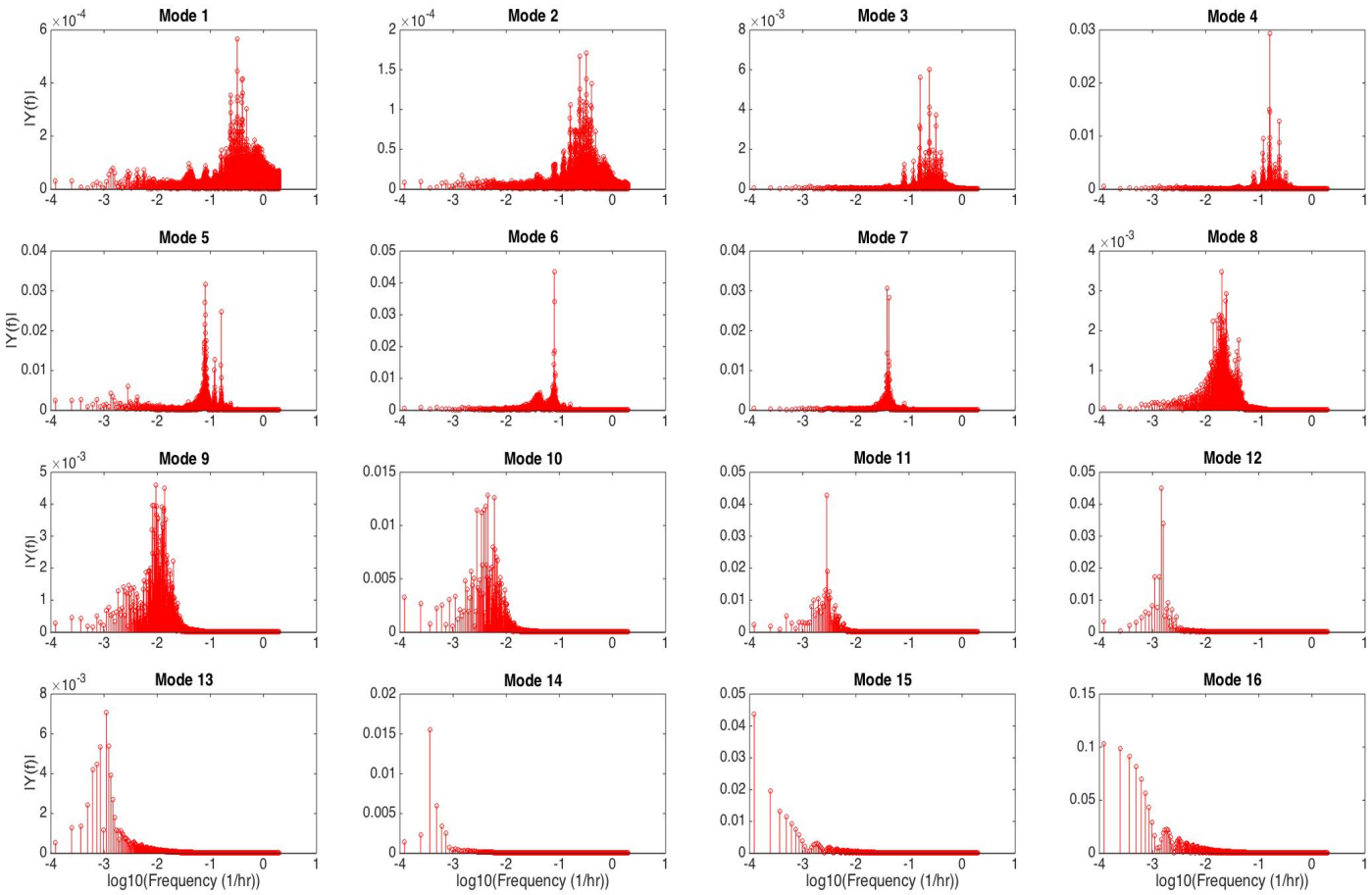

Figure 15. FFT on EMD Modes from Water Level Well 8: FFT results from each mode after water level at well 8 was run through an EMD.

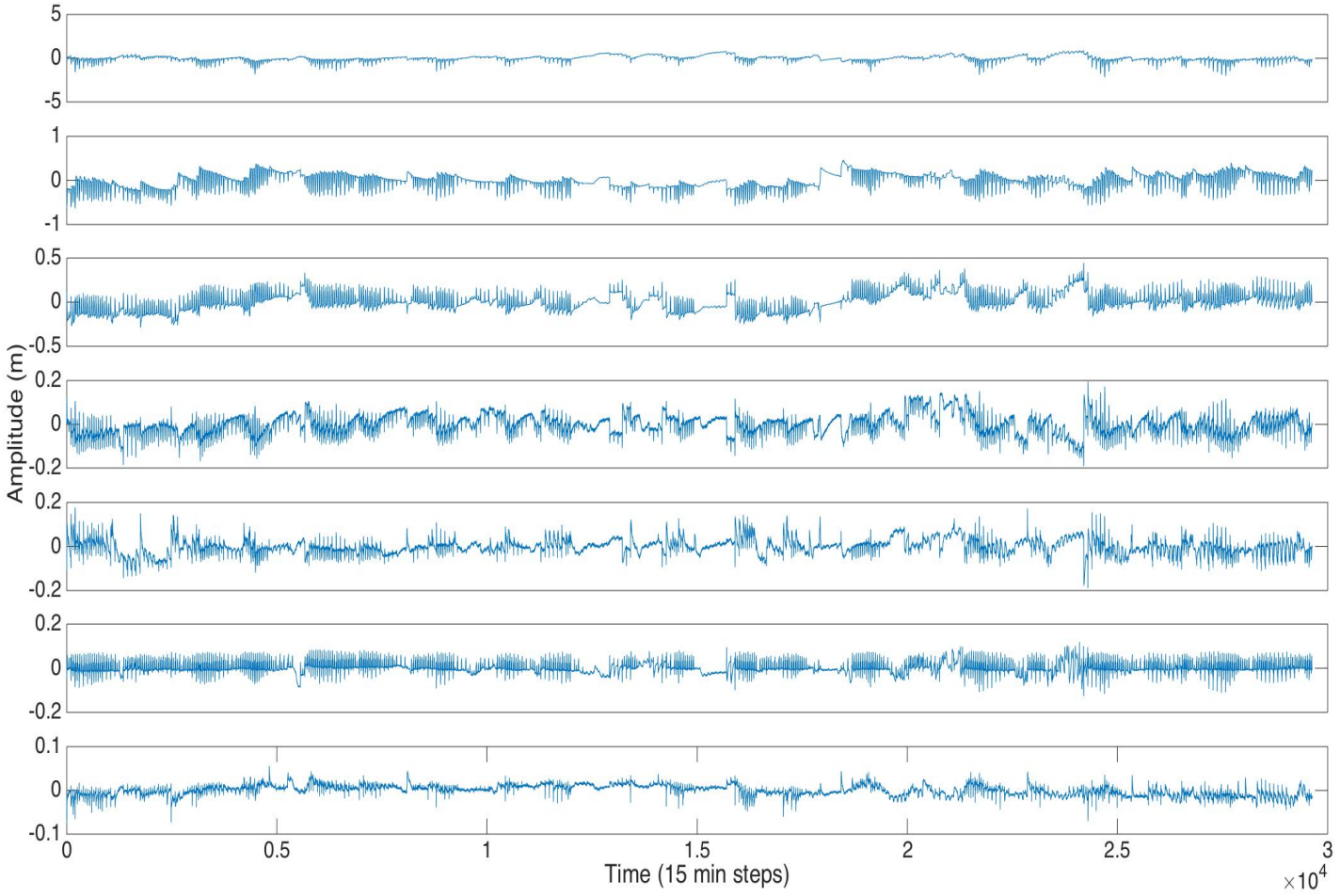

Figure 16. EOF Functions: Signals representing a function from EOF over time.

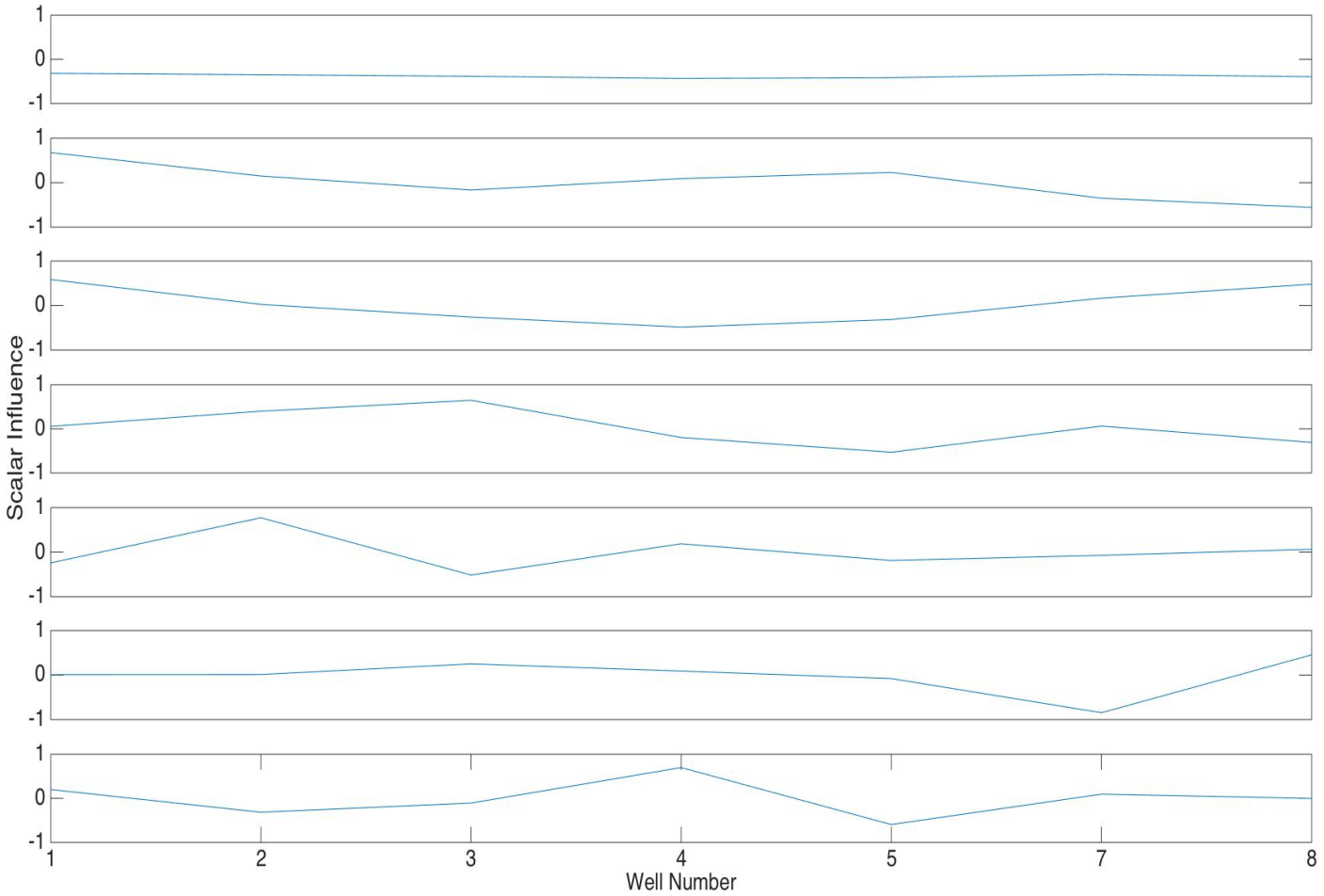

Figure 17. EOF Function Influence: Influence of each function based on well location.

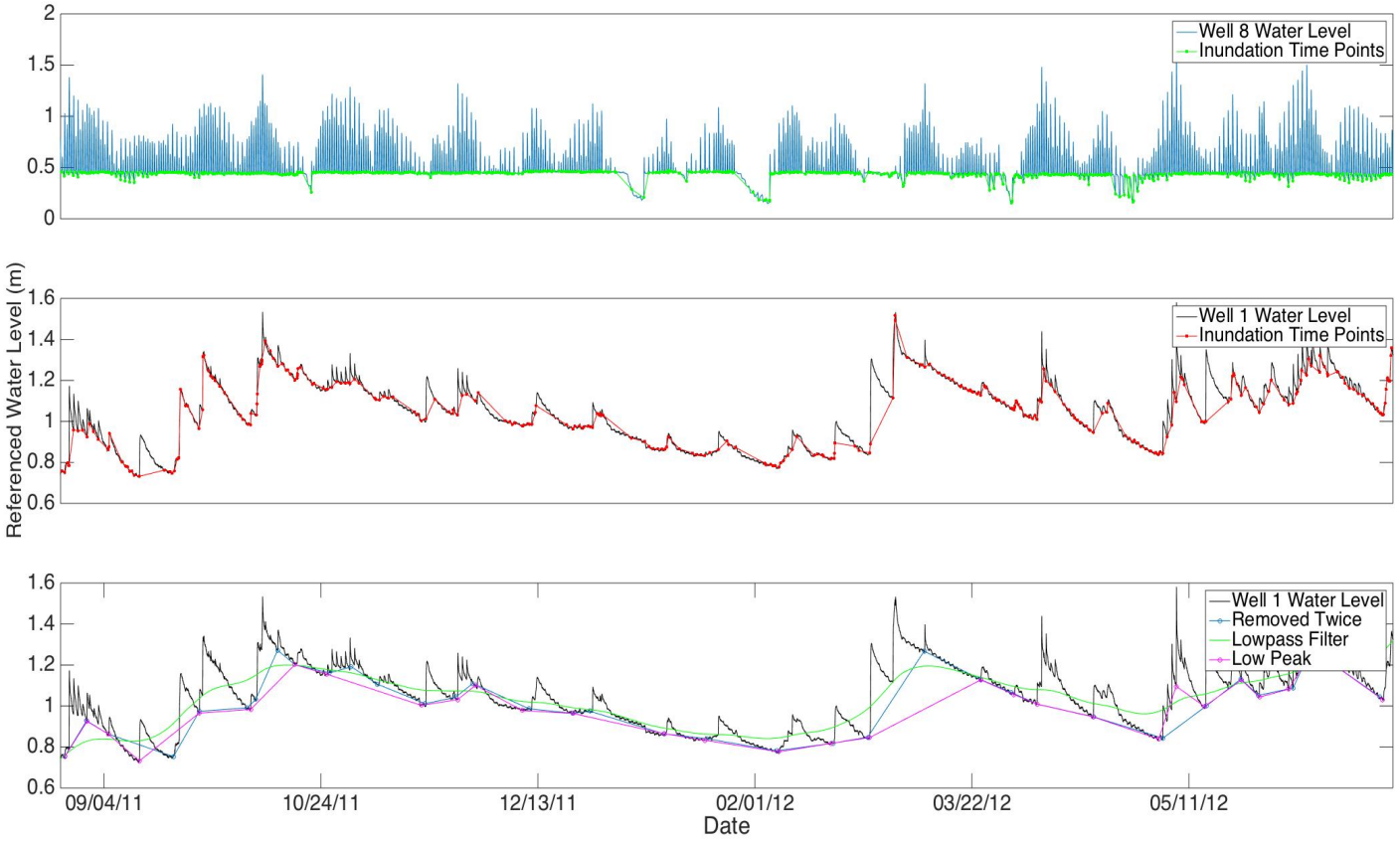

Figure 18. Removing Inundation for Well 1: Water level of well 8 (panel A-blue) and inundation (A-green). Water level of well 1 (B & C-black) and water level of well 1 with direct inundation removed (B-red). Three methods to remove tidal effect due to subsurface pressure waves (C-blue, green, and magenta).

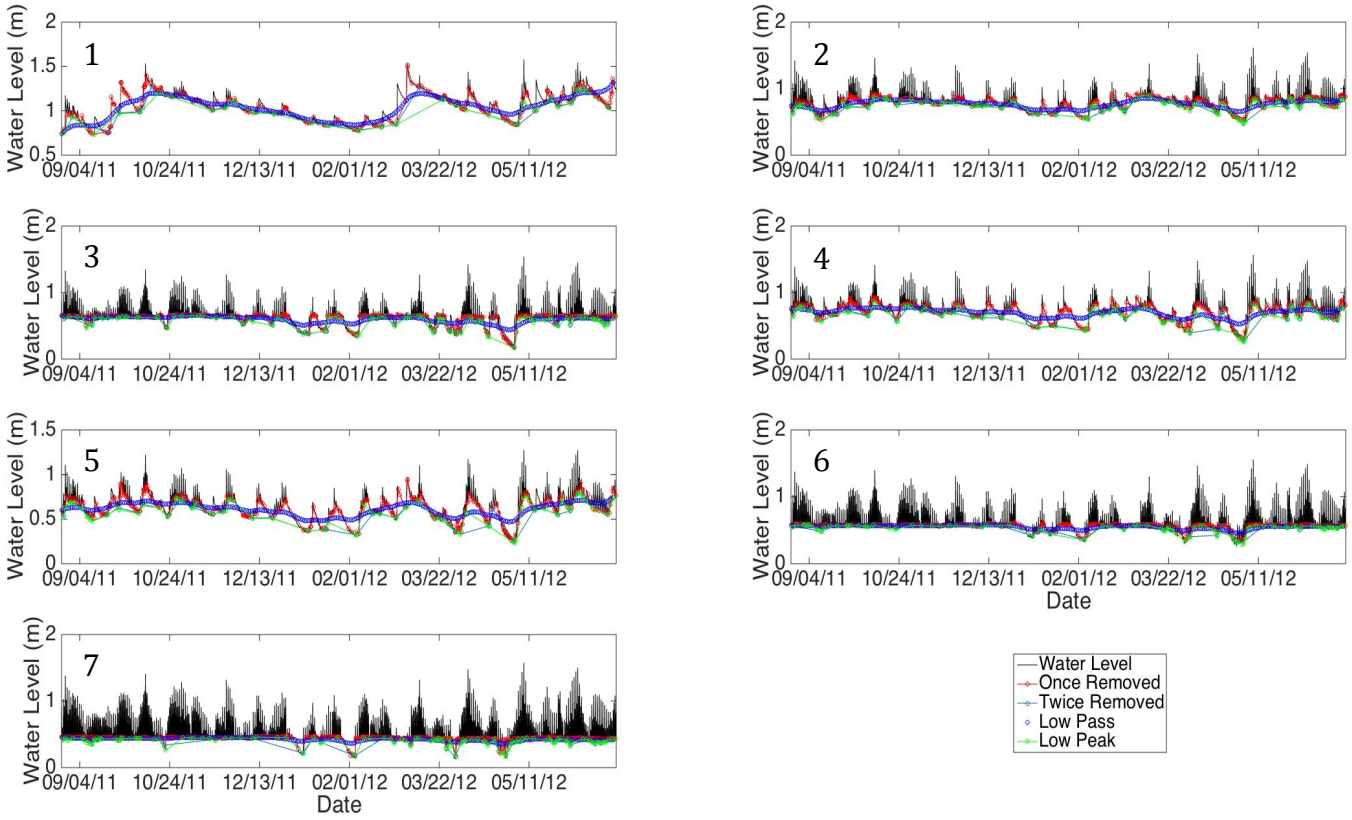

Figure 19. Three Methods for Removing Tidal Influence: Removing Tides using Inundation. Tidal influences are first removed through direct inundation (black). To remove the remaining tidal influences, three methods were implemented; twice removed (sky blue), low pass (blue circles), and low peak (green). Well number is indicated in upper left corner of the graph.

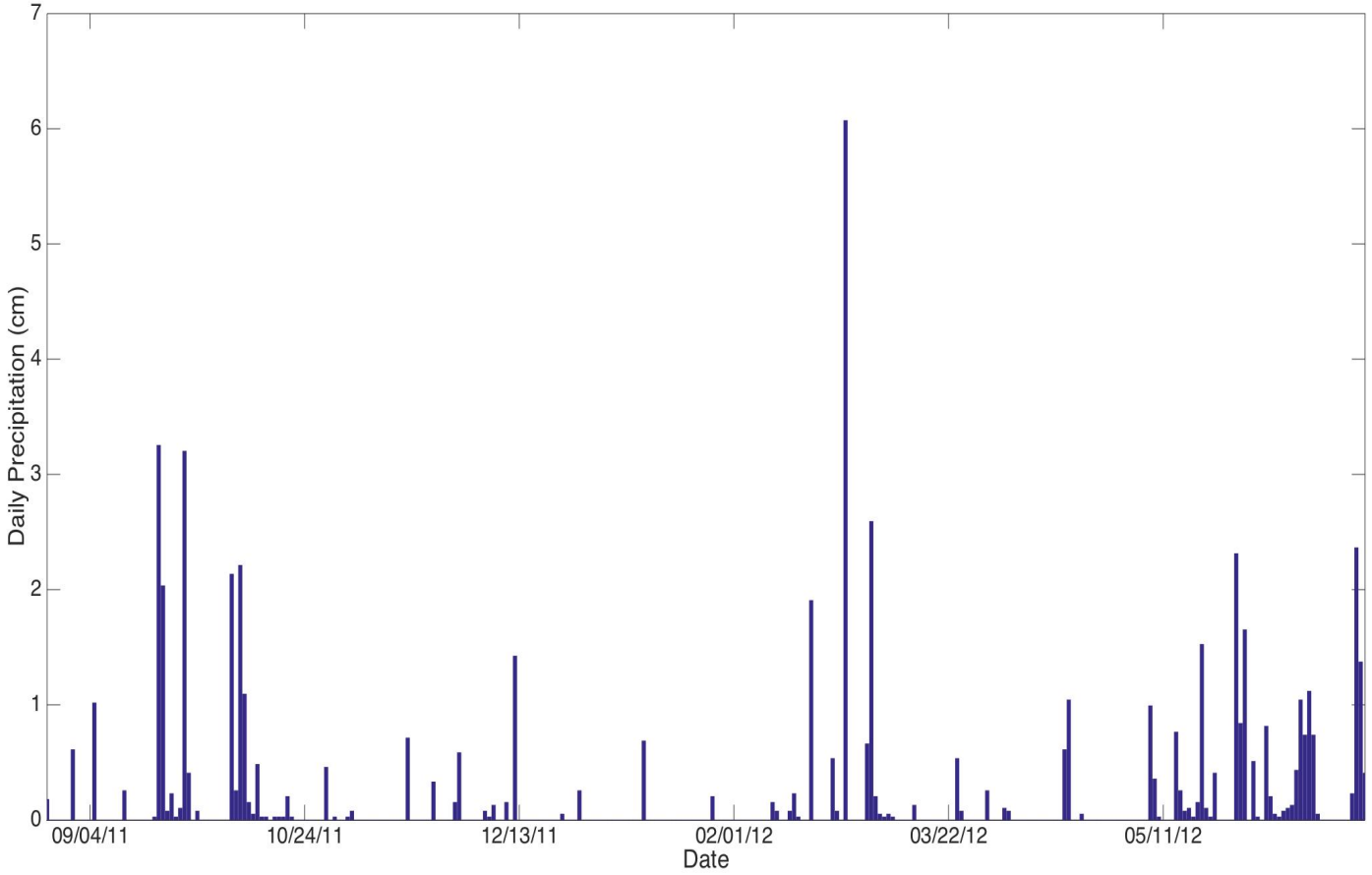

Figure 20. Daily precipitation in cm at Marsh Landing.

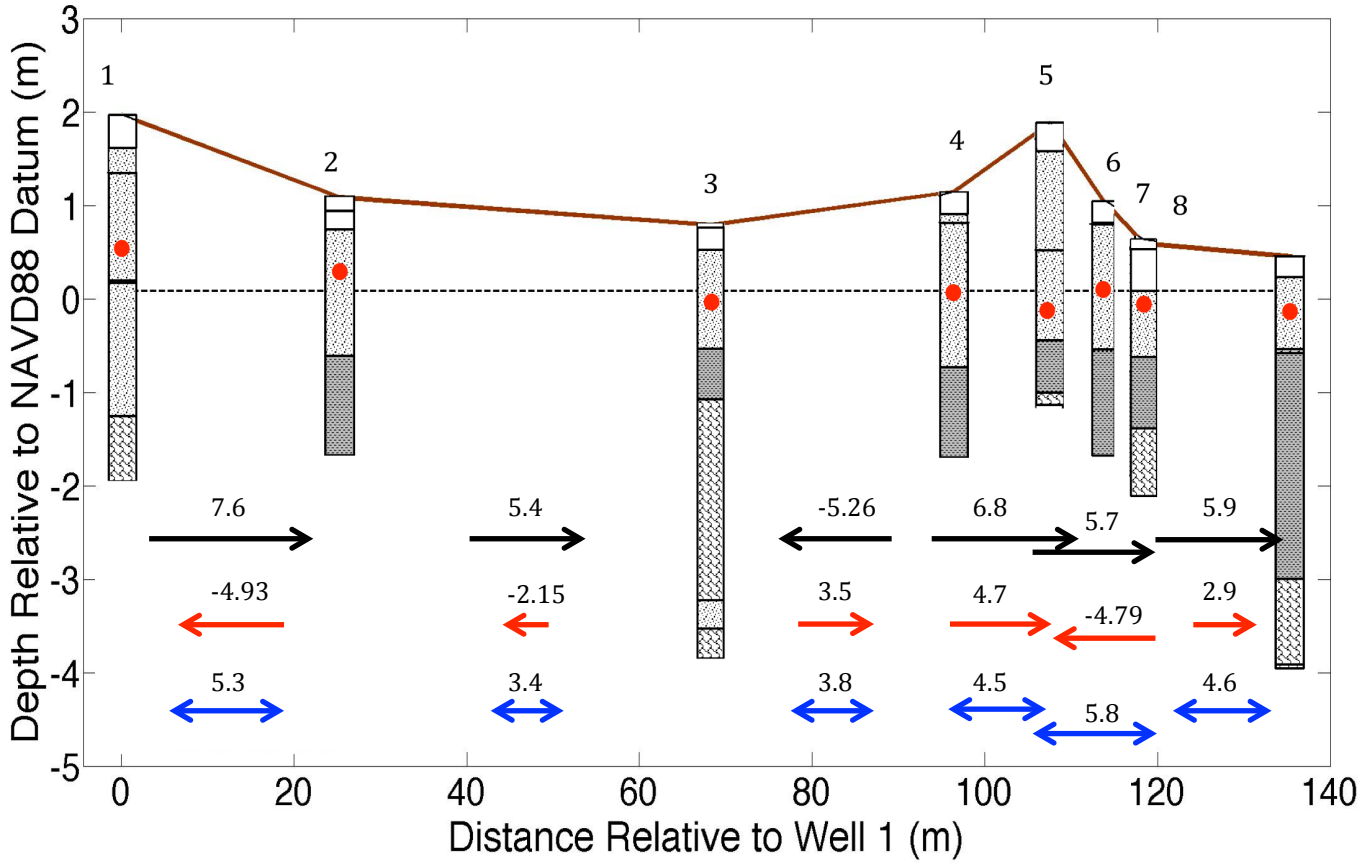

Figure 21. Contribution of Drivers: Average velocities (cm/yr) calculated for different drivers across the transect; total velocity (black), density driven flow (red), tidal inundation (blue). Arrow lengths reflect the natural logarithm of the velocities.

TABLES

Table 1. Piezometer Elevation Measurements at Hammock HN_i_1: Values recorded during installation of the wells to calculate elevations relative to NAVD88 datum (see Equation 2).

Well	Ground to well top (m; T)	Sensor to top of well (m)	Depth of well (m; DW)	Sonde distance from well bottom (m;B)	Height above sensor to ground (m;SG)	Sonde Elevation Relative to NAVD88 (m)
1	0.920	2.350	2.600	0.250	1.430	0.540
2	0.960	1.760	2.010	0.250	0.800	0.285
3	0.925	1.750	2.000	0.250	0.825	-0.035
4	0.970	2.040	2.290	0.250	1.070	0.074
5	1.090	3.070	3.470	0.400	1.980	-0.096
7	0.910	1.555	1.955	0.400	0.645	0.033
8	0.905	1.495	1.895	0.400	0.590	-0.141

Table 2. Average Darcy Velocities: Average velocities between the wells in m/s, the standard deviation, the maximum, and minimum velocities for all the well gradients.

Well Gradient	Average Velocity (m/s)	Standard Deviation	Maximum Velocity	Minimum Velocity
Wells 1 &2	6.64E-07	3.02E-07	1.49E-06	-1.23E-06
Wells 2 & 3	7.07E-08	3.44E-08	1.69E-07	-8.00E-08
Wells 3 &4	-6.09E-08	4.75E-08	2.39E-07	-2.05E-07
Wells 4 & 5	3.04E-07	1.07E-07	1.00E-06	-3.25E-08
Wells 5 &7	9.79E-08	3.33E-07	1.05E-06	-1.48E-06
Wells 7 & 8	1.24E-07	7.94E-08	3.50E-07	-2.65E-07

Table 3. Calculations for Permeability: Results from slug test used to calculate hydraulic conductivity and permeability.

Well #	1	8	3	5
T_o (s)	3.66E+01	1.12E+02	1.38E+02	7.93E+01
R/r (cm)	2.50E+00	2.50E+00	2.50E+00	2.50E+00
L (cm)	3.05E+01	3.05E+01	3.05E+01	3.05E+01
K (m/s)	7.00E-05	2.29E-05	1.86E-05	3.23E-05
Permeability (m^2)	7.00E-12	2.29E-12	1.86E-12	3.23E-12

Table 4. Average Pressure Gradient due to Density: Relative time averaged, absolute values of pressure gradients due to density (dps) and piezometric head (dph).

Well Gradients	$\frac{<\lvert dps/dx\rvert>}{<\lvert dph/dx\rvert>}$
Wells 1-2	0.06
Wells 2-3	0.03
Wells 3-4	0.16
Wells 4-5	0.13
Wells 5-7	0.09
Wells 7-8	0.10

Table 5. U_Tide Constituents from well 8 Water Level: U_Tide results on water level from well 8. Statistically significant constituents are indicated by * in front of the constituent name.

Constituent	Amplitude	Percent Energy	Signal to Noise
*M2	0.111	34.39%	2.60E+04
*M4	0.0635	11.35%	8.80E+03
*MSF	0.0558	8.76%	6.60E+03
*MM	0.0506	7.20%	5.30E+03
*S2	0.0412	4.77%	3.60E+03
*K1	0.0375	3.96%	2.90E+03
*N2	0.0369	3.82%	2.80E+03
*O1	0.0364	3.73%	2.80E+03
*MN4	0.0331	3.07%	2.40E+03
*SSA	0.0266	1.99%	1.40E+03
*MS4	0.0265	1.97%	1.50E+03
*MU2	0.0265	1.97%	1.50E+03
*MK3	0.0256	1.84%	1.40E+03
*M6	0.0236	1.57%	1.20E+03
*MO3	0.0213	1.28%	9.90E+02
*2MN6	0.0173	0.84%	6.50E+02
*MSM	0.0155	0.68%	5.00E+02
*MF	0.0151	0.64%	4.90E+02
*P1	0.0151	0.64%	4.80E+02
*MKS2	0.0148	0.61%	4.60E+02
*TAU1	0.0134	0.51%	3.80E+02
*NU2	0.0129	0.47%	3.50E+02
*EPS2	0.0128	0.46%	3.40E+02
*SO3	0.0113	0.36%	2.70E+02
*Q1	0.0112	0.35%	2.60E+02

*2MS6	0.0109	0.33%	2.50E+02
*L2	0.00983	0.27%	2.00E+02
*J1	0.00955	0.26%	1.90E+02
*LDA2	0.00945	0.25%	1.90E+02
*2MK5	0.00908	0.23%	1.80E+02
*MSN2	0.0083	0.19%	1.50E+02
*M3	0.0075	0.16%	1.20E+02
*M8	0.00722	0.15%	1.10E+02
*2N2	0.00575	0.09%	69
*OQ2	0.00547	0.08%	62
*PHI1	0.00544	0.08%	62
*SO1	0.00535	0.08%	61
*S4	0.00527	0.08%	59
*SIG1	0.00452	0.06%	43
*THE1	0.00451	0.06%	42
*ETA2	0.00396	0.04%	33
*SN4	0.00395	0.04%	34
*NO1	0.00387	0.04%	30
*SK3	0.00376	0.04%	31
*K2	0.00372	0.04%	29
*3MK7	0.00338	0.03%	25
*MK4	0.00319	0.03%	22
*2SM6	0.00294	0.02%	18
*2MK6	0.00284	0.02%	17
*SK4	0.00228	0.01%	11
*OO1	0.002	0.01%	8.5
*BET1	0.00198	0.01%	8.3
*ALP1	0.00141	0.01%	4.4
*MSK6	0.00104	0.00%	2.3
*2Q1	0.00103	0.00%	2.2
CHI1	0.000943	0.00%	1.8

RHO1	0.000742	0.00%	1.1
2SK5	0.00044	0.00%	0.42
UPS1	0.000428	0.00%	0.4

Table 6. U_Tide Constituents from well 8 Water Level Above Saturation: U_Tide results on water level above saturation from well 8. Statistically significant constituents are indicated by * in front of the constituent name.

Constituent	Amplitude	Percent Energy	Signal to Noise
*M2	0.13	13.42%	20
*K2	0.113	10.03%	62
*MN4	0.106	8.87%	42
*S2	0.098	7.61%	24
*MF	0.0968	7.42%	99
*N2	0.0863	5.89%	14
*MSF	0.0827	5.41%	27
*MM	0.0716	4.06%	14
*MS4	0.0676	3.62%	19
*K1	0.0673	3.58%	9.3
*MK4	0.0666	3.52%	28
*M6	0.0645	3.29%	22
*2N2	0.0608	2.93%	2.10E+02
*LDA2	0.0542	2.32%	18
*MU2	0.0488	1.88%	55
*M4	0.0481	1.83%	3.7
*MO3	0.0437	1.51%	41
*2MN6	0.043	1.46%	47
*NU2	0.0424	1.42%	38
*EPS2	0.0392	1.22%	2.60E+02
*2MK5	0.0368	1.07%	11
*MSN2	0.0315	0.78%	1.80E+02
*SSA	0.0291	0.67%	65
*NO1	0.0278	0.61%	33
*Q1	0.0273	0.59%	45

*2MK6	0.0265	0.55%	22
*O1	0.0255	0.51%	2.6
*M8	0.0227	0.41%	16
MK3	0.02	0.32%	1.5
*S4	0.0199	0.31%	46
*MKS2	0.0184	0.27%	27
*P1	0.0184	0.27%	5
MSM	0.0181	0.26%	1.5
*SN4	0.017	0.23%	7.1
*M3	0.0168	0.22%	17
*OQ2	0.0162	0.21%	59
*TAU1	0.0155	0.19%	8.7
*L2	0.0149	0.18%	3.1
*RHO1	0.0149	0.17%	14
*OO1	0.0104	0.09%	13
*SK4	0.0103	0.08%	11
*THE1	0.00986	0.08%	6.1
*PHI1	0.00977	0.08%	22
*SO3	0.00932	0.07%	3.6
*3MK7	0.00913	0.07%	3
*2Q1	0.00911	0.07%	9.5
*CHI1	0.00859	0.06%	5.2
*ALP1	0.00783	0.05%	16
*UPS1	0.00712	0.04%	16
*BET1	0.0068	0.04%	3.2
*ETA2	0.00652	0.03%	9.6
*2SM6	0.00642	0.03%	4.9
SO1	0.00621	0.03%	0.71
J1	0.00553	0.02%	1.8
SK3	0.00536	0.02%	1.4
MSK6	0.00421	0.01%	1.9

SIG1	0.00347	0.01%	0.55
2MS6	0.00248	0.00%	0.15
2SK5	0.0012	0.00%	0.46

Table 7. Precipitation vs. Tidally Removed Signal: Cross correlation between dh/dt and precipitation. Shown are maximum correlation coefficients, with the associated number of days over which the cumulative precipitation is compared to the water level changes in parentheses.

	Well Number	R value	R Value Standard Deviation	Lag	Lag Standard Deviation	Cumulative Days Past	Cumulative Days Past Standard Deviation)
Method 1	1	4.484E-01	1.486E-02	1.111E+00	1.023	8.611	1.852
	2	2.172E-01	6.510E-03	1.227E+01	7.301	14.90	6.599
	3	1.611E-01	4.926E-03	4.000E+01	0.817	3.000	1.414
	4	2.239E-01	1.142E-02	2.100E+01	0.000	3.000	1.000
	5	2.010E-01	5.998E-03	2.021E+01	1.437	17.58	5.157
	7	2.122E-01	6.573E-03	2.382E+01	2.377	10.76	3.569
	8	1.634E-01	7.199E-03	5.700E+01	0.000	2.000	1.000
Method 2	1	3.073E-01	9.241E-03	1.154E+01	3.563	18.89	2.751
	2	2.573E-01	9.595E-03	5.000E-01	0.577	3.000	0.817
	3	1.785E-01	5.308E-03	3.900E+01	0.000	2.500	0.707
	4	1.679E-01	5.459E-03	2.492E+01	3.118	7.083	5.744
	5	1.645E-01	5.521E-03	2.567E+01	2.807	8.750	6.047
	7	1.634E-01	4.341E-03	2.668E+01	1.157	13.79	5.442
	8	1.204E-01	3.875E-03	5.760E+01	63.65	2.000	1.225
Method 3	1	6.620E-01	2.065E-02	5.431E+00	3.624	13.57	4.435
	2	4.812E-01	1.419E-02	1.281E+01	4.382	16.84	3.238
	3	2.975E-01	9.220E-03	2.435E+01	2.194	15.68	2.500
	4	3.130E-01	9.204E-03	2.369E+01	2.850	17.29	2.583
	5	3.631E-01	9.561E-03	2.164E+01	3.264	17.44	2.395
	7	3.062E-01	9.161E-03	2.439E+01	2.032	15.97	3.002
	8	2.427E-01	7.478E-03	2.390E+01	1.758	16.41	2.450

Table 8: Displacement of water parcel over a tidal cycle: The influence of tide in terms of distance per semi-diurnal tide. A time-averaged window to average out tidal influence varies from M2 semi-diurnal tide to long-period components.

Well Gradient	1-2	2-3	3-4	4-5	5-7	7-8
Positive Water Levels Difference (m)	3.14E-02	3.12E-03	5.71E-05	1.24E-02	8.89E-03	5.49E-03
Negative Water Level Difference (m)	-2.05E-04	-1.48E-05	-3.04E-03	-4.41E-06	-3.41E-03	-1.60E-04
Positive M_2 (m)	1.35E-03	1.90E-04	3.33E-04	5.36E-04	2.94E-03	1.16E-03
Negative M_2 (m)	-1.35E-03	-1.90E-04	-3.32E-04	-5.35E-04	-2.94E-03	-1.16E-03
Positive Diurnal (m)	1.69E-03	2.40E-04	4.27E-04	6.98E-04	3.26E-03	1.27E-03
Negative Diurnal (m)	-1.69E-03	-2.40E-04	-4.26E-04	-6.97E-04	-3.27E-03	-1.28E-03
Positive 4 x M_2 (m)	1.88E-03	2.71E-04	4.75E-04	8.01E-04	3.37E-03	1.30E-03
Negative 4 x M_2 (m)	-1.89E-03	-2.71E-04	-4.74E-04	-7.99E-04	-3.37E-03	-1.30E-03
Positive Long-period Components (m)	2.98E-03	4.22E-04	6.86E-04	1.35E-03	4.64E-03	1.40E-03
Positive Long-period Components (m)	-2.99E-03	-4.23E-04	-6.89E-04	-1.34E-03	-4.63E-03	-1.40E-03

REFERENCES

Alexander, C. R., Smith, R. G., Calder, F. D., Schropp, S. J., & Windom, H. L. (1993). The Historical Record Of Metal Enrichment In 2 Florida Estuaries. *Estuaries, 16*(3B), 627-637. doi: 10.2307/1352800

Balugani, E., & Antonellini, M. (2011). Barometric pressure influence on water table fluctuations in coastal aquifers of partially enclosed seas: An example from the Adriatic coast, Italy. *Journal of Hydrology, 400*(1-2), 176-186. doi: 10.1016/j.jhydrol.2011.01.040

Bear, J. (1972). *Dynamics of Fluids in Porous Media*. New York: American Elsevier Publishing Co Inc.

Bellis, V. J. (1995). Ecology of maritime forests of the southern Atlantic coast: a community profile. *US Fish and Wildlife Service Biological Report, 30*, 1-95.

Bertness, M. D. (1991). Zonation Of Spartina-Patens And Spartina-Alterniflora In A New-England Salt-Marsh. *Ecology, 72*(1), 138-148. doi: 10.2307/1938909

Bertness, M. D., & Ellison, A. M. (1987). Determinants Of Pattern In A New-England Salt-Marsh Plant Community. *Ecological Monographs, 57*(2), 129-147. doi: 10.2307/1942621

Bertness, M. D., Ewanchuk, P. J., & Silliman, B. R. (2002). Anthropogenic modification of New England salt marsh landscapes. *Proceedings of the National Academy of Sciences of the United States of America, 99*(3), 1395-1398. doi: 10.1073/pnas.022447299

Blum, M. D., & Roberts, H. H. (2009). Drowning of the Mississippi Delta due to insufficient sediment supply and global sea-level rise. *Nature Geoscience, 2*(7), 488-491. doi: 10.1038/ngeo553

Boorman, L. A. (1999). Salt marshes - present functioning and future change. *Mangroves and Salt Marshes, 3*(4), 227-241.

Burnett, W. C., Bokuniewicz, H., Huettel, M., Moore, W. S., & Taniguchi, M. (2003). Groundwater and pore water inputs to the coastal zone. *Biogeochemistry, 66*(1-2), 3-33. doi: 10.1023/b:biog.0000006066.21240.53

Cacador, I. & Vale, C. (2001). Retention of heavy metals in salt marshes. In Prasad, M. N. V. (ed.), Metals in the environment: analysis by biodiversity. Marcel Dekker Inc., New York: 95-116.

Callaway, R. M., Jones, S., Ferren, W. R., & Parikh, A. (1990). Ecology Of A Mediterranean-Climate Estuarine Wetland At Carpinteria, California - Plant-Distributions And Soil-Salinity In The Upper Marsh. *Canadian Journal of Botany-Revue Canadienne De Botanique, 68*(5), 1139-1146.

Callaway, J. C., DeLaune, R. D., & Patrick, W. H. (1997). Sediment accretion rates from four coastal wetlands along the Gulf of Mexico. *Journal of Coastal Research, 13*(1), 181-191.

Chapman, V. J. (1974). *Salt Marshes And Salt Deserts Of The World*. 3-19.

Christiansen, T., Wiberg, P. L., & Milligan, T. G. (2000). Flow and sediment transport on a tidal salt marsh surface. *Estuarine Coastal and Shelf Science, 50*(3), 315-331. doi: 10.1006/ecss.2000.0548

Church, J. A., Gregory, J. M., Huybrechts, P., Kuhn, M., Lambeck, K., Nhuan, M. T.,

Qin, D., & Woodworth, P. L. (2001). Changes in sea level. Pages 639-693 in J. T. Houghton, Y. Ding, D. J. Griggs, M. Noguer, P. J. van der Linden, X. Dai, K Maskell, & C. A. Johnson, editors. Climate change 2001: the scientific basis. Contribution of working group I to the third assessment report of the intergovernmental panel on climate change. Cambridge University Press, Cambridge, UK.

Clarke, L. D., & Hannon, N. J. (1970). Mangrove Swamp And Salt Marsh Communities Of Sydney District .3. Plant Growth In Relation To Salinity And Waterlogging. *Journal of Ecology, 58*(2), 351-&. doi: 10.2307/2258276

Codiga, D.L., (2011). Unified Tidal Analysis and Prediction Using the UTide Matlab Functions. Technical Report 2011-01. Graduate School of Oceanography, University of Rhode Island, Narragansett, RI. 59pp. ftp://www.po.gso.uri.edu/pub/downloads/codiga/pubs/2011Codiga-UTide-Report.pdf

Comin, F. A., Romero, J. A., Astorga, V., & Garcia, C. (1997). Nitrogen removal and cycling in restored wetlands used as filters of nutrients for agricultural runoff. *Water Science and Technology, 35*(5), 255-261. doi: 10.1016/s0273-1223(97)00076-0

Cooper, A. (1982). The Effects Of Salinity And Waterlogging On The Growth And Cation Uptake Of Salt-Marsh Plants. *New Phytologist, 90*(2), 263-275. doi: 10.1111/j.1469-8137.1982.tb03258.x

Craft, C., Clough, J., Ehman, J., Joye, S., Park, R., Pennings, S., Guo, H. Y., Machmuller, M. (2009). Forecasting the effects of accelerated sea-level rise on

tidal marsh ecosystem services. *Frontiers in Ecology and the Environment, 7*(2), 73-78. doi: 10.1890/070219

Crites, R. W., Middlebrooks, E. J., & Reed, S. C. (2006). *Natural Wastewater Treatment Systems* (Vol. 19): CRC Press-Taylor & Francis Group.

Deegan, L. A., & Garritt, R. H. (1997). Evidence for spatial variability in estuarine food webs. *Marine Ecology Progress Series, 147*(1-3), 31-47. doi: 10.3354/meps147031

Diersch, H. J. G., & Kolditz, O. (2002). Variable-density flow and transport in porous media: approaches and challenges. *Advances in Water Resources, 25*(8-12), 899-944. doi: 10.1016/s0309-1708(02)00063-5

Doney, S. C., Ruckelshaus, M., Duffy, J. E., Barry, J. P., Chan, F., English, C. A., Galindo, H. M., Grebmeier, J. M., Hollowed, A. B., Knowlton, N., Polovina, J., Rabalais, N. N., Sydeman, W. J., Talley, L. D. (2012). Climate Change Impacts on Marine Ecosystems. *Annual Review of Marine Science, Vol 4, 4*, 11-37. doi: 10.1146/annurev-marine-041911-111611

Douglas, B. C., & Peltier, W. R. (2002). The puzzle of global sea-level rise. *Physics Today, 55*(3), 35-40. doi: 10.1063/1.1472392

Edwards, R. J., Wright, A., & Van de Plassche, O. (2004). Surface distributions of salt-marsh foraminifera from Connecticut, USA: modem analogues for high-resolution sea level studies. *Marine Micropaleontology, 51*(1-2), 1-21. doi: 10.1016/j.marmicro.2003.08.002

Ericson, J. P., Vorosmarty, C. J., Dingman, S. L., Ward, L. G., & Meybeck, M. (2006). Effective sea-level rise and deltas: Causes of change and human dimension

implications. *Global and Planetary Change, 50*(1-2), 63-82. doi: 10.1016/j.gloplacha.2005.07.004

Fofonoff, N. P., and Millard, R. C. Jr., 1983: Algorithms for computation of fundamental properties of seawater. Tech. Rep. 44, UNESCO, Technical Papers in Marine Science.

Freeze, R., and Cherry, J. (1979). *Groundwater*. Englewood Cliffs, New Jersey: Prentice-Hall.

Gardner, L. R. (2005). Role of geomorphic and hydraulic parameters in governing pore water seepage from salt marsh sediments. *Water Resources Research, 41*(7), 11. doi: 10.1029/2004wr003671

Gedan, K. B., Silliman, B. R., & Bertness, M. D. (2009). Centuries of Human-Driven Change in Salt Marsh Ecosystems. *Annual Review of Marine Science, 1*, 117-141. doi: 10.1146/annurev.marine.010908.163930

Glover, R. E. (1959). The pattern of freshwater flow in a coastal aquifer. J. Geophysics. Res., 64(4), 457-459.

Guha, H., & Panday, S. (2012). Impact of Sea Level Rise on Groundwater Salinity in a Coastal Community of South Florida. *Journal of the American Water Resources Association, 48*(3), 510-529. doi: 10.1111/j.1752-1688.2011.00630.x

Hackney, C. T., Burbanck, W. D., & Hackney, O. P. (1976). Biological And Physical Dynamics Of A Georgia Tidal Creek. *Chesapeake Science, 17*(4), 271-280. doi: 10.2307/1350514

Hammer, N. E., (1992). Designing constructed wetlands systems to treat agricultural nonpoint source pollution. *Ecological Engineering, 1*(1-2), 49-82. doi:10.1016/0925-8574(92)90025-W

Huang, N. E., Shen, Z., Long, S. R., Wu, M. L. C., Shih, H. H., Zheng, Q. N., Yen, N. C., Tung, C. C., Liu, H. H. (1998). The empirical mode decomposition and the Hilbert spectrum for nonlinear and non-stationary time series analysis. *Proceedings of the Royal Society A-Mathematical Physical and Engineering Sciences, 454*(1971), 903-995.

Huang, S. H., & Pant, H. K. (2009). Nitrogen transformation in wetlands and marshes. *Journal of Food Agriculture & Environment, 7*(3-4), 946-954.

Hughes, R. G. (2001). Biological and physical processes that affect saltmarsh erosion and saltmarsh restoration: Development of hypotheses. *Ecological Comparisons of Sedimentary Shores, 151*, 173-192.

Hughes, A. L. H., Wilson, A. M., & Morris, J. T. (2012). Hydrologic variability in a salt marsh: Assessing the links between drought and acute marsh dieback. *Estuarine Coastal and Shelf Science, 111*, 95-106. doi: 10.1016/j.ecss.2012.06.016

Isacch, J. P., Holz, S., Ricci, L., & Martinez, M. M. (2004). Post-fire vegetation change and bird use of a salt marsh in coastal Argentina. *Wetlands, 24*(2), 235-243. doi: 10.1672/0277-5212(2004)024[0235:pvcabu]2.0.co;2

Johnson, A.F. & Barbour, M.G. (1990) Dunes and maritime forests. Pages 429-480 in R.L. Myers and JJ Ewel, editors. Ecosystems of Florida. University Press of Florida, Gainesville. 765pp.

Kennish, M. J. (2001). Coastal salt marsh systems in the US: A review of anthropogenic

impacts. *Journal of Coastal Research, 17*(3), 731-748.

Li, H. L., Li, L., & Lockington, D. (2005). Aeration for plant root respiration in a tidal marsh. *Water Resources Research, 41*(6), 11. doi: 10.1029/2004wr003759

Loaiciga, H. A., Pingel, T. J., & Garcia, E. S. (2012). Sea Water Intrusion by Sea-Level Rise: Scenarios for the 21st Century. *Ground Water, 50*(1), 37-47. doi: 10.1111/j.1745-6584.2011.00800.x

Marani, M., Silvestri, S., Belluco, E., Ursino, N., Comerlati, A., Tosatto, O., & Putti, M. (2006). Spatial organization and ecohydrological interactions in oxygen-limited vegetation ecosystems. *Water Resources Research, 42*(6), 12. doi: 10.1029/2005wr004582

Martin J. (1996) Hydrology and pore-water chemistry of a tidal marsh, Fraser River estuary. MSc thesis, Simon Fraser University, 132 pp.

McCoy, C., Viso, R., Peterson, R. N., Libes, S., Lewis, B., Ledoux, J., Voulgaris, G., Smith, E., Sanger, D. (2011). Radon as an indicator of limited cross-shelf mixing of submarine groundwater discharge along an open ocean beach in the South Atlantic Bight during observed hypoxia. *Continental Shelf Research, 31*(12), 1306-1317. doi: 10.1016/j.csr.2011.05.009

Meile, C., Porubsky, W. P., Walker, R. L., & Payne, K. (2010). Natural attenuation of nitrogen loading from septic effluents: Spatial and environmental controls. *Water Research, 44*(5), 1399-1408. doi: 10.1016/j.watres.2009.11.019

Mendelssohn, I. A., & Morris, J. T. (2000). *Eco-physiological controls on the productivity of Spartina alterniflora Loisel*. Dordrecht: Springer pp 59-80.

Miller, L., & Douglas, B. C. (2004). Mass and volume contributions to twentieth-century

global sea level rise. *Nature, 428*(6981), 406-409. doi: 10.1038/nature02309

Morris, J. T., Sundareshwar, P. V., Nietch, C. T., Kjerfve, B., & Cahoon, D. R. (2002). Responses of coastal wetlands to rising sea level. *Ecology, 83*(10), 2869-2877. doi: 10.2307/3072022

Morzaria-Luna, H., Turk-Boyer, P., Rosemartin, A., & Camacho-Ibar, V. E. (2014). Vulnerability to climate change of hypersaline salt marshes in the Northern Gulf of California. *Ocean & Coastal Management, 93*, 37-50. doi: 10.1016/j.ocecoaman.2014.03.004

Nielsen, P. (1990). Tidal Dynamics of the Water Table in Beaches. *Water Recourse Research*, 26(9), 2127-2134.

Odum, W. E. (1988). Comparative Ecology Of Tidal Fresh-Water And Salt Marshes. *Annual Review of Ecology and Systematics, 19*, 147-176. doi: 10.1146/annurev.es.19.110188.001051

Pennings, S. C., & Callaway, R. M. (1992). Salt-Marsh Plant Zonation - The Relative Importance Of Competition And Physical Factors. *Ecology, 73*(2), 681-690. doi: 10.2307/1940774

Pennings, S. C., Grant, M. B., & Bertness, M. D. (2005). Plant zonation in low-latitude salt marshes: disentangling the roles of flooding, salinity and competition. *Journal of Ecology, 93*(1), 159-167. doi: 10.1111/j.1365-2745.2004.00959.x

Quintana, F., Guarracino, L., & Saliba, R. (2006). A numerical approach for groundwater flow in unsaturated porous media. *International Journal for Numerical Methods in Fluids, 51*(9-10), 1205-1215. doi: 10.1002/fld.1201

Rasmussen, T. C., & Crawford, L. A. (1997). Identifying and removing barometric

pressure effects in confined and unconfined aquifers. *Ground Water, 35*(3), 502-511. doi: 10.1111/j.1745-6584.1997.tb00111.x

Sanger, D. M., Holland, A. E., & Scott, G. I. (1999). Tidal creek and salt marsh sediments in South Carolina coastal estuaries: I. Distribution of trace metals. *Archives of Environmental Contamination and Toxicology, 37*(4), 445-457.

Schincariol, R. A., Schwartz, F. W., & Mendoza, C. A. (1994). On The Generation Of Instabilities In Variable-Density Flow. *Water Resources Research, 30*(4), 913-927. doi: 10.1029/93wr02951

Schultz, G., & Ruppel, C. (2002). Constraints on hydraulic parameters and implications for groundwater flux across the upland-estuary interface. *Journal of Hydrology, 260*(1-4), 255-269. doi: 10.1016/s0022-1694(01)00616-3

Shen, C., Jin, G., Xin, P., Kong, J., Li, L. (2015). Effects of salinity variations on pore-water flow in salt marshes. *Water Resources Research,* 'in press', doi: 10.1002/2015WR016911

Silliman, B. R., & Bertness, M. D. (2004). Shoreline development drives invasion of Phragmites australis and the loss of plant diversity on New England salt marshes. *Conservation Biology, 18*(5), 1424-1434. doi: 10.1111/j.1523-1739.2004.00112.x

Silva, H., Dias, J. M., & Cacador, I. (2009). Is the salt marsh vegetation a determining factor in the sedimentation processes? *Hydrobiologia, 621*, 33-47. doi: 10.1007/s10750-008-9630-7

Smith, A. J. (2004). Mixed convection and density-dependent seawater circulation in coastal aquifers. *Water Resources Research, 40*(8), 16. doi:

10.1029/2003wr002977

Stevenson, J. C., Kearney, M. S., & Pendleton, E. C. (1985). Sedimentation And Erosion In A Chesapeake Bay Brackish Marsh System. *Marine Geology, 67*(3-4), 213-235. doi: 10.1016/0025-3227(85)90093-3

Swarzenski, P. W., Simonds, F. W., Paulson, A. J., Kruse, S., & Reich, C. (2007). Geochemical and geophysical examination of submarine groundwater discharge and associated nutrient loading estimates into Lynch Cove, Hood Canal, WA. *Environmental Science & Technology, 41*(20), 7022-7029. doi: 10.1021/es070881a

Torres, M. E., Colominas, M. A., Schlotthauer, G., Flandrin, P., & Ieee. (2011). A Complete Ensemble Empirical Mode Decomposition With Adaptive Noise. *2011 Ieee International Conference on Acoustics, Speech, and Signal Processing*, 4144-4147.

Turck, J. A., & Alexander, C. R. (2013). Coastal Landscapes And Their Relationship To Human Settlement On The Georgia Coast. *Anthropological Papers of the American Museum of Natural History, 98*, 169-189.

Uddameri, V., Hernandez, E. A., & Estrada, F. (2014). A fuzzy simulation-optimization approach for optimal estimation of groundwater availability under decision maker uncertainty. *Environmental Earth Sciences, 71*(6), 2559-2572. doi: 10.1007/s12665-013-2905-y

Ursino, N., Silvestri, S., & Marani, M. (2004). Subsurface flow and vegetation patterns in tidal environments. *Water Resources Research, 40*(5), 11. doi: 10.1029/2003wr002702

Vince, S. W., & Snow, A. A. (1984). Plant Zonation In An Alaskan Salt-Marsh .1. Distribution, Abundance And Environmental-Factors. *Journal of Ecology, 72*(2), 651-667. doi: 10.2307/2260074

Wang, T., Zhang, M., Yu, Q., & Zhang, H. (2012). Comparing the applications of EMD and EEMD on time–frequency analysis of seismic signal. *Journal of Applied Geophysics, 83*, 29-34. doi: 10.1016/j.jappgeo.2012.05.002

Wenner, E. L., & Beatty, H. R. (1993). Utilization Of Shallow Estuarine Habitats In South-Carolina, USA, By Postlarval And Juvenile Stages Of Penaeus Spp (Decapoda, Penaeidae). *Journal of Crustacean Biology, 13*(2), 280-295. doi: 10.2307/1548975

Werner, A. D., & Simmons, C. T. (2009). Impact of Sea-Level Rise on Sea Water Intrusion in Coastal Aquifers. *Ground Water, 47*(2), 197-204. doi: 10.1111/j.1745-6584.2008.00535.x

Wilson, A. M., & Gardner, L. R. (2006). Tidally driven groundwater flow and solute exchange in a marsh: Numerical simulations. *Water Resources Research, 42*(1), 9. doi: 10.1029/2005wr004302

Wilson, A. M., Huettel, M., & Klein, S. (2008). Grain size and depositional environment as predictors of permeability in coastal marine sands. *Estuarine Coastal and Shelf Science, 80*(1), 193-199. doi: 10.1016/j.ecss.2008.06.011

Xin, P., Yuan, L. R., Li, L., & Barry, D. A. (2011). Tidally driven multiscale pore water flow in a creek-marsh system. *Water Resources Research, 47*, 19. doi: 10.1029/2010wr010110

Yuan, L. R., Xin, P., Kong, J., Li, L., & Lockington, D. (2011). A coupled model for

simulating surface water and groundwater interactions in coastal wetlands. *Hydrological Processes, 25*(23), 3533-3546. doi: 10.1002/hyp.8079

Zhang, H., & Gorelick, S. M. (2014). Coupled impacts of sea-level rise and tidal marsh restoration on endangered California clapper rail. *Biological Conservation, 172*, 89-100. doi: 10.1016/j.biocon.2014.02.016

APPENDIX

```
%% Section 1: EMD SCRIPT

% script to analyze timeseries using elementary mode decomposition (emd)
% and empirical orthognal functions (eof)
% oct 17, 2014

% read in the data
% sapelo sound pressure time series
% Date: matlab date
% Depth: water depth in m
% Pressure: pressure in dbar
load('sap_sound.mat')
load('corrected_data_elevations_cleaned.mat')

% description of corrected_data_elevations
% % input data
% p(nwell,time): measured pressure in each well in Pa
% S(nwell,time): measured salinity in g/kg
% T(nwell,time): measured temp in degC
% zm(nwell): measured sensor depth in m, NAVD88
% pos(nwell): location of well in m (to compute horizonatal distance)
% well(nwell): well index, denoting the relative sequence of wells
% tday: time in days
%
% % derived quantities
% rho(nwell,time): density in kg/m3 computed as f(p,S,T)
% pr(nwell,time): pressure at reference depth in Pa
% zref: reference depth in m
% hr(nwell,time): head relative to reference depth in m

% havg(time): average head between two adjacent wells in Pa
% rhoavg(time): average density between two adjacent wells in kg/m3
% dph(time): difference in head component of pressure between adjacent wells
in Pa
% dps(time): difference in density component of pressure between adjacent
wells in Pa
% r_htos(nwell-1,time): ratio of head vs. density driven flow between
adjacent wells

% constants
g=9.81; % gravitational acceleration in m/s2

% data

well=[1 2 3 4 5 7 8]; % to keep track which well the pressure data is coming
from
nwell = size(well,2);

perm_slug(1,1) = 7.00293E-12; % Result from slug test well 1
```

```
perm_slug(1,2) = 1.86138E-12; % Result from slug test well 3
perm_slug(1,3) = 3.23186E-12; % Result from slug test well 5
perm_slug(1,4) = 2.2943E-12; % Result from slug test well 8

% derived data
zref          = mean(mean(zm));         % average sensor depth in m, NADV88
used as reference depth
pressure      = p.*(1/1000000);         % convert measured pressure (Pa) into
compatible units for function (dbars)
[SVAN, SIGMA] = swstate(S,T,pressure);  % uses the WHOI Oceans Tool box
function swstate to provide a density anomoly
rho           = SIGMA + 1000;           % must add 1000 to convert the
density anaomoly to density (kg/m3)
u             = 10.^(-3).*(1+1.551.*10.^(-2).*(T-20)).^(-1.572)-
6.8138.*10.^(-7)*S+5.263.*10.^(-5); % Viscosity in Pa*s
pr            = p+rho.*g.*(zm-zref);    % Pressure at referenced sonde depth
hr            = pr./rho./g;             % water level at referenced sonde
depth

for i=1:nwell-1
    havg(:,i)     = (hr(:,i+1)+hr(:,i))/2;              % head average for
each well throughout time
    rhoavg(:,i)   = (rho(:,i+1)+rho(:,i))/2;            % density average
for each well throughout time
    dph(:,i)      = (rhoavg(:,1).*g.*(hr(:,i+1)-hr(:,i))./pos(i); % The
partial change in pressure due to piezometric head changes
    dps(:,i)      = (havg(:,1).*g.*(rho(:,i+1)-rho(:,i))./pos(i); % The
partial change in pressure due to density changes associated with temperature
and salinty changes
    pgrad(:,i)    = (pr(:,i+1)-pr(:,i))./pos(i);        % Pressure gradient
between wells
    u_avg(:,i)    = (u(:,i+1)+u(:,i))/2;
end

    q(:,1)    = -perm_slug(:,1)./u_avg(:,1).*pgrad(:,1);
    q(:,2)    = -perm_slug(:,2)./u_avg(:,2).*pgrad(:,2);
    q(:,3)    = -perm_slug(:,2)./u_avg(:,3).*pgrad(:,3);
    q(:,4)    = -perm_slug(:,3)./u_avg(:,4).*pgrad(:,4);
    q(:,5)    = -perm_slug(:,3)./u_avg(:,5).*pgrad(:,5);
    q(:,6)    = -perm_slug(:,4)./u_avg(:,6).*pgrad(:,6);

    q_den(:,1)    = -perm_slug(:,1)./u_avg(:,1).*dps(:,1);
    q_den(:,2)    = -perm_slug(:,2)./u_avg(:,2).*dps(:,2);
    q_den(:,3)    = -perm_slug(:,2)./u_avg(:,3).*dps(:,3);
    q_den(:,4)    = -perm_slug(:,3)./u_avg(:,4).*dps(:,4);
    q_den(:,5)    = -perm_slug(:,3)./u_avg(:,5).*dps(:,5);
    q_den(:,6)    = -perm_slug(:,4)./u_avg(:,6).*dps(:,6);

% estimate tidal components in Sapelo Sound using U_Tide
% http://www.po.gso.uri.edu/~codiga/utide/utide.htm

% establish tidal coefficients
coef1 = ut_solv(Date, Pressure, [], 32, 'auto', 'NodsatNone','White','OLS',
'LinCI');

% reconstruct time series data
% [sl_fit, ~ ] = ut_reconstr(Date,coef1);
```

```
% EMD of Sapelo Sound signal
dt = Date(3,1)-Date(2,1); % in days
dt = dt*24; % dt in hours
x  = Pressure;

Nstd = 0.05; % noise standard deviation
NR   = 10; % number of realizations
MaxIter = 10;% maximum number of sifting iterations allowed.

[modes its]=ceemdan(x,Nstd,NR,MaxIter);
figure,
subplot(2,1,1), plot(sum(modes)), hold on, plot(x,'k.'), legend ('sum modes',
'true signal')
subplot(2,1,2), plot(modes'), title('modes')

% identify the frequencies in the modes using FFT
for i=1:size(modes,1)
    L = size(modes,2);
    Fs=1/dt;
    NFFT = 2^nextpow2(L);
    f = Fs/2*linspace(0,1,NFFT/2+1);
    Yfilt = fft(modes(i,:),NFFT)/L;
    figure
    stem(f,2*abs(Yfilt(1:NFFT/2+1)),'r')
    xlabel('Frequency (1/hr)'), ylabel('|Y(f)|')
end

% find the peaks
signal=2*abs(Yfilt(1:NFFT/2+1));
[maxLoc, maxMag] = peakfinder(signal,[],[], 1,0);

figure, strips(modes'), title(['EEMD result tide level']);

% Running Well 8 signal through empirical mode decomposition (EMD)
x=hr(:,7);
NR=100;
[modes its]=ceemdan(x,Nstd,NR,MaxIter);
figure,
subplot(2,1,1), plot(sum(modes)), hold on, plot(x,'k.'), legend ('sum modes',
'true signal')
subplot(2,1,2), plot(modes'), title('modes')

% Plot
figure;
plot(tday, modes'), hold on
    xlabel('Date'),...
    ylabel('Water Level'),...
    datetick('x','mm/dd/yy','keeplimits','keepticks'),...
    xlim([min(tday) max(tday)])

dt = tday(2,1)-tday(1,1); % in days
dt = dt*24; % dt in hours

% Run an FFT
for i=1:size(modes,1)
```

```
    L = size(modes,2);
    Fs=1/dt;
    NFFT = 2^nextpow2(L);
    f = Fs/2*linspace(0,1,NFFT/2+1);
    Yfilt = fft(modes(i,:),NFFT)/L;
    figure
    stem(f,2*abs(Yfilt(1:NFFT/2+1)),'r')
    xlabel('Frequency (1/hr)'), ylabel('|Y(f)|')

end

% Run an FFT
figure
for i=1:size(modes,1)
    L = size(modes,2);
    Fs=1/dt;
    NFFT = 2^nextpow2(L);
    f = Fs/2*linspace(0,1,NFFT/2+1);
    Yfilt = fft(modes(i,:),NFFT)/L;
    subplot(4,4,i), ...
    stem(log10(f),2*abs(Yfilt(1:NFFT/2+1)),'r')
    xlabel('log10(Frequency (1/hr))'), ylabel('|Y(f)|'), title(['Mode ',
num2str(i)])
end

% find the peaks
signal=2*abs(Yfilt(1:NFFT/2+1));
[maxLoc, maxMag] = peakfinder(signal,[],[], 1,0);

figure, strips(modes'), title(['EEMD result well8']);

%% EOF of well transect
% cut into monthly pieces, else the matrix is too big
% S=pr(1:2880,:)';
% S=pr';
Q=hr(1:29632,:)';
% remove average
Snew=Q-mean(Q')'*ones(1,size(Q,2));
[eve,eva,amp]=rmc_eof_SVD(Snew);
% eve(locations, modes)
% amp(time,mode)

% figure, plot(eve(:,imode)) % plot mode i at all locations
% figure, plot(amp(:,imode)) % plot amplitude of mode 1 over time
eva(1:size(eva,1))/sum(eva)*100 % variance explained in modes
nmodes=7
figure
for imode=1:nmodes
    subplot(nmodes,1,imode), plot(eve(:,imode)) % plot mode i at all
locations
end
xlabel('mode vs. location')

figure
for imode=1:nmodes
    subplot(nmodes,1,imode), plot(amp(:,imode)) % plot mode i at all
locations
```

```
end
xlabel('amplitude for each mode vs. time (in 15 min steps)')

% reconstruct mode i over time
iloc=1; % location index
imode=2; % mode index
% show the impact of mode over time at all wells
figure
for iloc=1:7
reconst = mean(Q(imode,:))  + eve(iloc,imode)*amp(:,imode);
% to compare mode, consider amp/std(amp) and eve = eve*std(amp)

subplot(7,1,iloc),plot(reconst)
end

dt = tday(2,1)-tday(1,1); % in days
dt = dt*24; % dt in hours

% do FFT on amp
for i=1:size(amp,2)
    L = size(amp,1);
    Fs=1/dt;
    NFFT = 2^nextpow2(L);
    f = Fs/2*linspace(0,1,NFFT/2+1);
    Yfilt = fft(amp(:,i),NFFT)/L;
    figure
    stem(f,2*abs(Yfilt(1:NFFT/2+1)),'r')
    xlabel('Frequency (1/hr)'), ylabel('|Y(f)|')
end

%% Section 2 Inundation

% Using Well 8 as an inundation meter
% identify incoming tide in well 8
L = length(hr(:,1)); % number of points in pressure time series
counter= 0 ;
dpthresh = 0.0059; % threshold that defines relevant change in pressure for
well 8
ntide = 7; % well 8
for i=2:L-1
    if hr(i+1,ntide)-hr(i,ntide)> dpthresh % dp in well 8 greater than
dpthresh
        if hr(i,ntide)-hr(i-1,ntide)> dpthresh
        else

            counter = counter+1;
            p_removed(counter,ntide) = hr(i,ntide); % pressure
            t_removed(counter,ntide) = tday(i,1); % time
            n_removed(counter)=i; % index

        end
    end
end
nctot(ntide)=counter; % number of points in reduced timeseries

for nw=1:6 % loop over wells
```

```
    nc=0; % counter for each well
    for i=1:counter-1 % go from segment to segment
        pcrit = hr(n_removed(i),nw); % water level in well X must exceed
water level in well 8 at tide start
        ind=n_removed(i); % actual index in time series
        while ind<n_removed(i+1) % steps over each point
            if(hr(ind+1,nw)>(pcrit+dpthresh)) % ?????
                nc=nc+1;
                p_removed(nc,nw)=hr(ind,nw);
                t_removed(nc,nw)=tday(ind,1);
                ind = n_removed(i+1);
            else
                ind=ind+1;
            end
            [nw nc ind]
        end
    end
    nctot(nw)=nc;
end

% lowpass filter of all tide signals: 30-hr Butterworth, low-pass filter
% see http://stackoverflow.com/questions/13570306/matlab-butterworth
nb = 1; % filter order
fs = 0.0011;     % sample frequency; 1/15min = 0.0011 Hz
fc = 9.2593e-06; % cutoff frequency; 1/30hr  = 9.2593e-06 Hz
dataIn = hr(:,7);
[b,a] = butter(nb, fc/(fs/2));
y = filtfilt(b,a,dataIn); %// output

% correlation with precipitation

% read in precipitation data
% Date_011_2012: Date in matlab time number (days)
% Precipitation: Daily totals of precipitation (cm)
load('Precip.mat'); % read in Date_2011_2012, Precipitation
Precipitation(80)=0;

% interpolate well data to precipitation data
iw=7;
for iw=1:7

    method = 'linear';
    yi =
interp1(t_removed(1:nctot(iw),iw),p_removed(1:nctot(iw),iw),Date_2011_2012,me
thod,'extrap');
    h_interp(:,iw)=yi;
    clear yi
end

% remove S/N using lowpass filter
nb = 1; % filter order
fs = 0.0011;     % sample frequency; 1/15min = 0.0011 Hz
fc = 2.4802e-05; % cutoff frequency; 1/(2*14day)in Hz
for iw=1:7
    dataIn = h_interp(:,iw);
    [b,a] = butter(nb, fc/(fs/2));
    y = filtfilt(b,a,dataIn); %// output
```

```
    h_interp_filt(:,iw)=y;
end

% low peakfind
for iw=1:7
    x0=p_removed(1:nctot(iw),iw);
    sel=(max(x0)-min(x0))/4;
    sel = sel/10;
    [peakLoc,peakMag] = peakfinder(x0,sel,[],-1);
    nn(iw)=size(peakLoc,1);
    timep(1:nn(iw),iw)=t_removed(peakLoc,iw);
    hpeak(1:nn(iw),iw)=peakMag;
end

% remove S/N using threshold
for ntide =1:7
    L = length(h_interp(:,ntide)); % number of points in pressure time series
    counter= 0 ;
    dpthresh = 0.0059; % threshold that defines relevant change in pressure
    for i=2:L-1
        if h_interp(i+1,ntide)-h_interp(i,ntide)> dpthresh % dp in well 8
greater than dpthresh
            if h_interp(i,ntide)-h_interp(i-1,ntide)> dpthresh
            else
                counter = counter+1;
                p_removed2(counter,ntide) = h_interp(i,ntide); % pressure
                t_removed2(counter,ntide) = Date_2011_2012(i,1); % time
                n_removed2(counter)=i; % index

            end
        end
    end
    nctot2(ntide)=counter;
end

% visualize
X_MIN = min(tday);
X_MAX = max(tday);

figure,
for iw=1:7
    subplot(4,2,iw)
    plot(tday,hr(:,iw),'k'), hold on, ...
        %         plot(Date_2011_2012,h_interp(:,iw),'r.'), hold on, ...
    plot(t_removed(1:nctot(iw),iw),p_removed(1:nctot(iw),iw),'ro-'), hold on,
    plot(t_removed2(1:nctot2(iw),iw),p_removed2(1:nctot2(iw),iw),'o-'), hold
on, ... % good
        plot(Date_2011_2012,h_interp_filt(:,iw),'bo'), hold on, ...
        plot(timep(1:nn(iw),iw),hpeak(1:nn(iw),iw),'go-'), hold on, ... %
good
        xlim([X_MIN X_MAX])
        legend('Water Level','Once Removed','Twice Removed','Low Pass','Low
Peak'), ...
        xlabel('Date'),ylabel('Water Level (m)')
        datetick('x','mm/dd/yy','keeplimits','keepticks'),...
end
```

```
% interpolate the good signals to daily values

method = 'linear';

for iw=1:7
    % signal using removed twice
    yi =
interp1(t_removed2(1:nctot2(iw),iw),p_removed2(1:nctot2(iw),iw),Date_2011_201
2,method,'extrap');
    hrr_interp(:,iw)=yi;

    % signal using removed once then lowpeak
    yi =
interp1(timep(1:nn(iw),iw),hpeak(1:nn(iw),iw),Date_2011_2012,method,'extrap')
;
    hrp_interp(:,iw)=yi;
end

% Precip
% Removing weighted signals
% correlate with precipiation over 1 to trange days
trange = 21; % days back to consider precip
L = size(Date_2011_2012,1);

        icccc=0;

for window=1:trange
    w0 = ones(size(1:trange));        % equal weight
    for t=window:L
        precw0(t) = sum(w0(1:window)' .* Precipitation(t-window+1 : t));
    end
    % indices for precip > 0
    indw0_pos=(precw0>0);

    % loop over all wells
    for iw=1:7

        % compute cross correlation between precip and water level
        % and save the lag for the one with the highest correlation
        y = h_interp_filt(window:L,iw);
        [r,lag] = xcorr(precw0(window:L),y,'coeff');
        rsave=r; r = (lag>0 | lag==0).*r;
        lagrlw0(window,iw) = lag(r==max(r)); rrlw0(window,iw)=max(r); clear r
lag
        clear y

        y = hrr_interp(window:L,iw);
        [r,lag] = xcorr(precw0(window:L),y,'coeff');
        rsave=r; r = (lag>0 | lag==0).*r;
        lagrrw0(window,iw) = lag(r==max(r)); rrrw0(window,iw)=max(r); clear r
lag
        clear y

        y = hrp_interp(window:L,iw);
        [r,lag] = xcorr(precw0(window:L),y,'coeff');
        rsave=r; r = (lag>0 | lag==0).*r;
```

```
        lagrpw0(window,iw) = lag(r==max(r)); rrpw0(window,iw)=max(r); clear r
lag
        clear y

        % compute cross correlation between precip and water level for data
point with precip > 0
        if(window>1)
            iii=logical(indw0_pos.*[zeros(1,window) ones(1,L-
window)].*[1:L]);
        else
            iii=logical(indw0_pos.*ones(1,L).*[1:L]);
        end

        y = h_interp_filt(iii,iw);
        [r,lag] = xcorr(precw0(iii),y,'coeff');
        rsave=r; r = (lag>0 | lag==0).*r;
        zlagrlw0(window,iw) = lag(r==max(r)); zrrlw0(window,iw)=max(r); clear
r lag
        clear y

        y = hrr_interp(iii,iw);
        [r,lag] = xcorr(precw0(iii),y,'coeff');
        rsave=r; r = (lag>0 | lag==0).*r;
        zlagrrw0(window,iw) = lag(r==max(r)); zrrrw0(window,iw)=max(r); clear
r lag
        clear y

        y = hrp_interp(iii,iw);
        [r,lag] = xcorr(precw0(iii),y,'coeff');
%         rsave=r; r = (lag>0).*r;
        rsave=r; r = (lag>0 | lag==0).*r;
        zlagrpw0(window,iw) = lag(r==max(r)); zrrpw0(window,iw)=max(r); clear
r lag
        clear y

        % run correlation on dh/dt vs. precip
        y = h_interp_filt(window+1:L,iw) -  h_interp_filt(window:L-1,iw);
        [r,lag] = xcorr(precw0(window+1:L),y,'coeff');

for iii=1:size(r,2)
    icccc=icccc+1;
    rrr(icccc)=r(iii);
    lll(icccc)=lag(iii);
    www(icccc)=window;
    iww(icccc)=iw;
    mmm(icccc)=3;
end

        rsave=r; r = (lag>0 | lag==0).*r;
        dlagrlw0(window,iw) = lag(r==max(r)); drrlw0(window,iw)=max(r); clear
r lag
         clear y

        y = hrr_interp(window+1:L,iw) -  hrr_interp(window:L-1,iw);
        [r,lag] = xcorr(precw0(window+1:L),y,'coeff');
for iii=1:size(r,2)
    icccc=icccc+1;
```

```
    rrr(icccc)=r(iii);
    lll(icccc)=lag(iii);
    www(icccc)=window;
    iww(icccc)=iw;
    mmm(icccc)=1;
end
        rsave=r; r = (lag>0 | lag==0).*r;
        dlagrrw0(window,iw) = lag(r==max(r)); drrrw0(window,iw)=max(r); clear
r lag
        clear y

        y = hrp_interp(window+1:L,iw) - hrp_interp(window:L-1,iw);
        [r,lag] = xcorr(precw0(window+1:L),y,'coeff');
for iii=1:size(r,2)
    icccc=icccc+1;
    rrr(icccc)=r(iii);
    lll(icccc)=lag(iii);
    www(icccc)=window;
    iww(icccc)=iw;
    mmm(icccc)=2;
end

        rsave=r; r = (lag>0 | lag==0).*r;
        dlagrpw0(window,iw) = lag(r==max(r)); drrpw0(window,iw)=max(r); clear
r lag
        clear y;

        [window iw]
    end

    clear w0 w1 w2 precw0 precw1 precw2

end

% execute this for each well and each method by chaning iww and mmm
keep = ( ((lll>0) | (lll==0)) );
keep2 = ( (iww==7) & (mmm==3) );
rrrall= rrr(logical(keep.*keep2));
rcrit = max(rrrall)*0.9;
keep3 = (rrr>rcrit);
tt=logical(keep.*keep2.*keep3);
rkept = mean(rrr(tt))
rkeptstd = std(rrr(tt))
lagkept = mean(lll(tt))
lagkeptstd = std(lll(tt))
cumkept = mean(www(tt))
cumkeptstd = std(www(tt))

% Visulization

figure;
    plot(tday(:,1),hr(:,7)), hold on

plot(t_removed(1:nctot(7),7),p_removed(1:nctot(7),7),'g','MarkerSize',10,'Mar
ker','.')
    plot(tday(:,1),hr(:,1),'b'), hold on
```

```
plot(t_removed(1:nctot(1),1),p_removed(1:nctot(1),1),'r','MarkerSize',10,'Mar
ker','.')

% Figures
X_MIN = [734740;]
X_MAX = [735047;]
iw = 1;
figure;
subplot(4,1,1)
    plot(tday(:,1),hr(:,7)), hold on
        xlim([X_MIN X_MAX])
        datetick('x','mm/dd/yy','keeplimits','keepticks'),...
        xlabel('Date'),ylabel('Referenced Water Level (m)')

plot(t_removed(1:nctot(7),7),p_removed(1:nctot(7),7),'g','MarkerSize',10,'Mar
ker','.')
        xlim([X_MIN X_MAX])
        datetick('x','mm/dd/yy','keeplimits','keepticks'),...
        legend('Well 8 Water Level','Inundation Time Points'), ...
subplot(4,1,2)
    plot(tday(:,1),hr(:,1),'k'), hold on
        xlim([X_MIN X_MAX])
        xlabel('Date'),ylabel('Referenced Water Level (m)')
        datetick('x','mm/dd/yy','keeplimits','keepticks'),...

plot(t_removed(1:nctot(1),1),p_removed(1:nctot(1),1),'r','MarkerSize',10,'Mar
ker','.')
            xlim([X_MIN X_MAX])
            datetick('x','mm/dd/yy','keeplimits','keepticks'),
            legend('Well 1 Water Level','Inundation Time Points'), ...
subplot(4,1,3)
    plot(tday,hr(:,iw),'k'), hold on, ...
            xlim([X_MIN X_MAX])
            xlabel('Date'),ylabel('Referenced Water Level (m)')
            datetick('x','mm/dd/yy','keeplimits','keepticks'),...
    plot(t_removed2(1:nctot2(iw),iw),p_removed2(1:nctot2(iw),iw),'o-'), hold
on, ...
            xlim([X_MIN X_MAX])
            datetick('x','mm/dd/yy','keeplimits','keepticks'),...
        plot(Date_2011_2012,h_interp_filt(:,iw),'g'), hold on,
            xlim([X_MIN X_MAX])
            datetick('x','mm/dd/yy','keeplimits','keepticks'),...
        plot(timep(1:nn(iw),iw),hpeak(1:nn(iw),iw),'mo-'), hold on, ...
            xlim([X_MIN X_MAX])
            datetick('x','mm/dd/yy','keeplimits','keepticks'),...
            legend('Well 1 Water Level','Removed Twice','Lowpass Filter','Low
Peak'), ...
subplot(4,1,4)
    bar(Date_2011_2012, Precipitation)
        xlim([X_MIN X_MAX])
        datetick('x','mm/dd/yy','keeplimits','keepticks'),
        xlabel('Date'),ylabel('Daily Precipitation (cm/yr)')

% Precipitation removed figure

X_MIN = [734740;]
X_MAX = [735047;]
iw = 1;
```

```
figure;
subplot(3,1,1)
    plot(tday(:,1),hr(:,7)), hold on
        xlim([X_MIN X_MAX])
        datetick('x','mm/dd/yy','keeplimits','keepticks'),...
        xlabel('Date'),ylabel('Referenced Water Level (m)')

plot(t_removed(1:nctot(7),7),p_removed(1:nctot(7),7),'g','MarkerSize',10,'Mar
ker','.')
        xlim([X_MIN X_MAX])
        datetick('x','mm/dd/yy','keeplimits','keepticks'),...
        legend('Well 8 Water Level','Inundation Time Points'), ...
subplot(3,1,2)
    plot(tday(:,1),hr(:,1),'k'), hold on
        xlim([X_MIN X_MAX])
        xlabel('Date'),ylabel('Referenced Water Level (m)')
        datetick('x','mm/dd/yy','keeplimits','keepticks'),...

plot(t_removed(1:nctot(1),1),p_removed(1:nctot(1),1),'r','MarkerSize',10,'Mar
ker','.')
            xlim([X_MIN X_MAX])
            datetick('x','mm/dd/yy','keeplimits','keepticks'),
            legend('Well 1 Water Level','Inundation Time Points'), ...
subplot(3,1,3)
    plot(tday,hr(:,iw),'k'), hold on, ...
            xlim([X_MIN X_MAX])
            xlabel('Date'),ylabel('Referenced Water Level (m)')
            datetick('x','mm/dd/yy','keeplimits','keepticks'),...
    plot(t_removed2(1:nctot2(iw),iw),p_removed2(1:nctot2(iw),iw),'o-'), hold
on, ...
            xlim([X_MIN X_MAX])
            datetick('x','mm/dd/yy','keeplimits','keepticks'),...
        plot(Date_2011_2012,h_interp_filt(:,iw),'g'), hold on,
            xlim([X_MIN X_MAX])
            datetick('x','mm/dd/yy','keeplimits','keepticks'),...
        plot(timep(1:nn(iw),iw),hpeak(1:nn(iw),iw),'mo-'), hold on, ...
            xlim([X_MIN X_MAX])
            datetick('x','mm/dd/yy','keeplimits','keepticks'),...
            legend('Well 1 Water Level','Removed Twice','Lowpass Filter','Low
Peak'), ...

% Poster Quality figure for zoomed in look
X_MIN = [734869;]
X_MAX = [734929;]

iw = 1;
figure;

subplot(2,1,1)
    plot(tday(:,1),hr(:,1),'k'), hold on
        xlim([X_MIN X_MAX])
        xlabel('Date'),ylabel('Referenced Water Level (m)')
        datetick('x','mm/dd/yy','keeplimits','keepticks'),...

plot(t_removed(1:nctot(1),1),p_removed(1:nctot(1),1),'r','MarkerSize',10,'Mar
ker','.')
            xlim([X_MIN X_MAX])
            datetick('x','mm/dd/yy','keeplimits','keepticks'),
```

```
            legend('Well 1 Water Level','Inundation Time Points'), ...
subplot(2,1,2)

plot(t_removed(1:nctot(1),1),p_removed(1:nctot(1),1),'r','MarkerSize',10,'Mar
ker','.'), hold on
            xlim([X_MIN X_MAX])
            datetick('x','mm/dd/yy','keeplimits','keepticks'),...
    plot(t_removed2(1:nctot2(iw),iw),p_removed2(1:nctot2(iw),iw),'o-'), hold
on ...
            xlim([X_MIN X_MAX])
            datetick('x','mm/dd/yy','keeplimits','keepticks'),...
        plot(Date_2011_2012,h_interp_filt(:,iw),'g'), hold on,
            xlim([X_MIN X_MAX])
            datetick('x','mm/dd/yy','keeplimits','keepticks'),...
        plot(timep(1:nn(iw),iw),hpeak(1:nn(iw),iw),'mo-'), hold on, ...
            xlim([X_MIN X_MAX])
            datetick('x','mm/dd/yy','keeplimits','keepticks'),...
            legend('Well 1 Water Level','Removed Twice','Lowpass Filter','Low
Peak')

% Poster Quality figures
X_MIN = [734740;]
X_MAX = [735047;]
iw = 1;
figure;
subplot(4,1,1)
    plot(tday(:,1),hr(:,7)), hold on
        xlim([X_MIN X_MAX])
        datetick('x','mm/dd/yy','keeplimits','keepticks'),...
        xlabel('Date'),ylabel('Referenced Water Level (m)')

plot(t_removed(1:nctot(7),7),p_removed(1:nctot(7),7),'g','MarkerSize',10,'Mar
ker','.')
        xlim([X_MIN X_MAX])
        datetick('x','mm/dd/yy','keeplimits','keepticks'),...
        legend('Well 8 Water Level','Inundation Time Points'), ...
subplot(4,1,2)
    plot(tday(:,1),hr(:,1),'k'), hold on
        xlim([X_MIN X_MAX])
        xlabel('Date'),ylabel('Referenced Water Level (m)')
        datetick('x','mm/dd/yy','keeplimits','keepticks'),...

plot(t_removed(1:nctot(1),1),p_removed(1:nctot(1),1),'r','MarkerSize',10,'Mar
ker','.')
            xlim([X_MIN X_MAX])
            datetick('x','mm/dd/yy','keeplimits','keepticks'),
            legend('Well 1 Water Level','Inundation Time Points'), ...
subplot(4,1,3)

plot(t_removed(1:nctot(1),1),p_removed(1:nctot(1),1),'r','MarkerSize',10,'Mar
ker','.'), hold on
            xlim([X_MIN X_MAX])
            datetick('x','mm/dd/yy','keeplimits','keepticks'),...
    plot(t_removed2(1:nctot2(iw),iw),p_removed2(1:nctot2(iw),iw),'o-'), hold
on ...
            xlim([X_MIN X_MAX])
            datetick('x','mm/dd/yy','keeplimits','keepticks'),...
        plot(Date_2011_2012,h_interp_filt(:,iw),'g'), hold on,
```

```
            xlim([X_MIN X_MAX])
            datetick('x','mm/dd/yy','keeplimits','keepticks'),...
        plot(timep(1:nn(iw),iw),hpeak(1:nn(iw),iw),'mo-'), hold on, ...
            xlim([X_MIN X_MAX])
            datetick('x','mm/dd/yy','keeplimits','keepticks'),...
            legend('Well 1 Water Level','Removed Twice','Lowpass Filter','Low
Peak'), ...
subplot(4,1,4)
    bar(Date_2011_2012, Precipitation)
        xlim([X_MIN X_MAX])
        datetick('x','mm/dd/yy','keeplimits','keepticks'),
        xlabel('Date'),ylabel('Daily Precipitation (cm/yr)')

% Two graphs for GCE

% 4 Graph Breakdown
    % Remove 2nd Graph
    % Run same graph for all the wells

X_MIN = [734740;]
X_MAX = [735047;]
iw = 1;
figure;
subplot(3,1,1)
    plot(tday(:,1),hr(:,7)), hold on
        xlim([X_MIN X_MAX])
        datetick('x','mm/dd/yy','keeplimits','keepticks'),...
        xlabel('Date'),ylabel('Referenced Water Level (m)')

plot(t_removed(1:nctot(7),7),p_removed(1:nctot(7),7),'g','MarkerSize',10,'Mar
ker','.')
        xlim([X_MIN X_MAX])
        datetick('x','mm/dd/yy','keeplimits','keepticks'),...
        legend('Well 8 Water Level','Inundation Time Points'), ...
subplot(3,1,2)
    plot(tday(:,1),hr(:,1),'k'), hold on
            xlim([X_MIN X_MAX])
            datetick('x','mm/dd/yy','keeplimits','keepticks'),...
    plot(t_removed2(1:nctot2(iw),iw),p_removed2(1:nctot2(iw),iw),'o-'), hold
on ...
            xlim([X_MIN X_MAX])
            datetick('x','mm/dd/yy','keeplimits','keepticks'),...
            legend('Removed Once','Removed Twice'), ...
subplot(3,1,3)
    bar(Date_2011_2012, Precipitation)
        xlim([X_MIN X_MAX])
        datetick('x','mm/dd/yy','keeplimits','keepticks'),
        xlabel('Date'),ylabel('Daily Precipitation (cm/yr)')

% zoomed in look
X_MIN = [734869;]
X_MAX = [734929;]

iw = 1;
figure;

subplot(2,1,1)
```

```
    plot(tday(:,1),hr(:,1),'k'), hold on
        xlim([X_MIN X_MAX])
        xlabel('Date'),ylabel('Referenced Water Level (m)')
        datetick('x','mm/dd/yy','keeplimits','keepticks'),...

plot(t_removed(1:nctot(1),1),p_removed(1:nctot(1),1),'r','MarkerSize',10,'Mar
ker','.')
            xlim([X_MIN X_MAX])
            datetick('x','mm/dd/yy','keeplimits','keepticks'),
            legend('Well 1 Water Level','Removed Once'), ...
subplot(2,1,2)

plot(t_removed(1:nctot(1),1),p_removed(1:nctot(1),1),'r','MarkerSize',10,'Mar
ker','.'), hold on
            xlim([X_MIN X_MAX])
            datetick('x','mm/dd/yy','keeplimits','keepticks'),...
    plot(t_removed2(1:nctot2(iw),iw),p_removed2(1:nctot2(iw),iw),'o-'), hold
on ...
            xlim([X_MIN X_MAX])
            datetick('x','mm/dd/yy','keeplimits','keepticks'),...
            legend('Removed Once','Removed Twice'), ...

% Looking at water level gradients with tide removed in comparison

% step 1 Compute water level gradient
for i=1:nwell-1
    hrgrad(:,i)    = (hr(:,i+1)-hr(:,i))./pos(i);         % Water Level
gradient between wells

end

% Conduct gradients on tide removed signals
for i=1:nwell-1
    hrgradmethod1(:,i)    = (hr(:,i+1)-hr(:,i))./pos(i);         % Water
Level gradient between tide removed mthd 1
    hrgradmethod2(:,i)    = (hr(:,i+1)-hr(:,i))./pos(i);         % Water
Level gradient between tide removed mthd 2
    hrgradmethod3(:,i)    = (hr(:,i+1)-hr(:,i))./pos(i);         % Water
Level gradient between tide removed mthd 3
end

%% Figures looking at comparisons

figure;
plot(tday(:,1),hr(:,1)), hold on
plot(t_removed2(1:37,1),p_removed2(1:37,1)), hold on
plot(t_removed(1:307,1),p_removed(1:307,1))

figure;
plot(tday(:,1),hr(:,7)), hold on
plot(t_removed2(1:47,7),p_removed2(1:47,7)), hold on
plot(t_removed(:,7),p_removed(:,7))

figure;
plot(tday(:,1),hr(:,7)), hold on
plot(tday(:,1),hr(:,6)), hold on
plot(t_removed2(1:46,6),p_removed2(1:46,6)), hold on
```

```
plot(t_removed2(1:47,7),p_removed2(1:47,7)), hold on

figure;
plot(tday(:,1),hr(:,1)), hold on
plot(tday(:,1),hr(:,2)), hold on
plot(t_removed2(1:37,1),p_removed2(1:37,1)), hold on
plot(t_removed2(1:53,2),p_removed2(1:53,2)), hold on

figure;
plot(tday(:,1),hr(:,3)), hold on
plot(tday(:,1),hr(:,2)), hold on
plot(t_removed2(1:64,3),p_removed2(1:64,3)), hold on
plot(t_removed2(1:53,2),p_removed2(1:53,2)), hold on

figure;
plot(tday(:,1),hr(:,4)), hold on
plot(tday(:,1),hr(:,3)), hold on
plot(t_removed2(1:48,4),p_removed2(1:48,4)), hold on
plot(t_removed2(1:64,3),p_removed2(1:64,3)), hold on

figure;
plot(tday(:,1),hr(:,5)), hold on
plot(tday(:,1),hr(:,4)), hold on
plot(t_removed2(1:41,5),p_removed2(1:41,5)), hold on
plot(t_removed2(1:48,4),p_removed2(1:48,4)), hold on

figure;
plot(tday(:,1),hr(:,6)), hold on
plot(tday(:,1),hr(:,5)), hold on
plot(t_removed2(1:46,6),p_removed2(1:46,6)), hold on
plot(t_removed2(1:41,5),p_removed2(1:41,5)), hold on




%% Moving Average to Remove Tidal influences

% http://www.mathworks.com/matlabcentral/fileexchange/41859-moving-average-
function

% compute h_avg
% in: h: measured values
% h_avg: running mean of measured values, timewindow = M2

idx1=6;
idx2=idx1+1;
% dh= h_wll2-h_well1
dhcm = hr(:,idx2)-hr(:,idx1);

%dhavg=h_avg_wll2-h_avg_well1
% window = (12*60+25)/15;
window = 49;
h_avg = movingmean(hr,window);
dh_avg_cm1 = h_avg(:,idx2)-h_avg(:,idx1);
```

```
window = 99;
h_avg = movingmean(hr,window);
dh_avg_cm2 = h_avg(:,idx2)-h_avg(:,idx1);

window = 1345;
h_avg = movingmean(hr,window);
dh_avg_cm3 = h_avg(:,idx2)-h_avg(:,idx1);

figure,
plot(dhcm), hold on,
plot(dh_avg_cm1,'r'), hold on
plot(dh_avg_cm2,'m'), hold on
plot(dh_avg_cm3,'g')

% Plot salinity
figure14 = figure;
    plot(tday,S), hold on
    xlabel('Date'),...
    ylabel('Salinity (g/kg)'),...
    datetick('x','mm/dd/yy','keeplimits','keepticks')
    xlim([min(tday) max(tday)])

% Plotting Precipitation

figure;
bar(Date_2011_2012, Precipitation)
        xlim([X_MIN X_MAX])
        datetick('x','mm/dd/yy','keeplimits','keepticks'),
        xlabel('Date'),ylabel('Daily Precipitation (cm/day)')

%% Plotting Darcy velocities

 figure;
    plot(tday,q), hold on
    xlabel('Date'),...
    ylabel('Darcy Velocity (m/s)'),...
    datetick('x','mm/dd/yy','keeplimits','keepticks')
    xlim([min(tday) max(tday)])
%% Section 3 Propagation

% Back Calculating Tidal Propagation with know Hydraulic Condutivity values
%Created 11/3/11 by John Ledoux

% Test for the tidal signal
t=(1:60:100000);
y=4.2+(.75.*cos(((2.*pi.*t)./43200)+(pi./2)));
plot(t,y)

% Equation for h(x,t)
% Variables
x=(1:1000);             % Distance in meters
t=(1:100:100000);       % Time in seconds
b=4.2;                  % Base line for water level in meters
A=.75;                  % Amplitude of Tidal Signal in meters
w=((2.*pi)./43200);     % Angular frequency
I=(pi./2);              % Phase shift
```

```
% Assumptions
S=.2;           % Storativity (unitless)
K=10.^-5;       % Hydraulic Conductivity in m*s^-1 (Mathidle's thesis)
T=K*b;          % Calculated Transmisivity
D=T/S;          % Calculated Diffusivity

% Equations
EQ1=(w./(2.*D));
EQ2=(-x.*(sqrt(EQ1)));
EQ3=(exp(EQ2));
EQ4=((w.*t)-I-EQ2);
EQ5=cos(EQ4);

% Equation at time t
h=b+A.*EQ3.*EQ5;

% With mesh (3D Plot)

x=(1:100);                  % Distance in meters
t=(1:60:86400);             % Time step in seconds (every minute for 24 hours
or two full tidal cycles)
[X,TM]=meshgrid(x,t);       % Creat mesh for x,y,z plot
b=1.5;                      % Base line for water level in meters. Acquired
from Mathilde's Thesis
A=.75;                      % Amplitude of Tidal Signal in meters. Acquired
from Mathilde's Thesis
w=((2.*pi)./43200);         % Angular frequency. Acquired from Mathilde's
Thesis
I=(pi./2);                  % Phase shift. Acquired from Mathilde's Thesis


% Assumptions
S=.02;           % Storativity (unitless). Acquired from Schultz % Ruppel
K=2.29*10.^-5;       % Hydraulic Conductivity in m*s^-1 Well 8
%K=7.0029*10.^-5;       % Hydraulic Conductivity in m*s^-1 Well 1
T=K*b;          % Calculated Transmisivity (Value = 4.2*10^-4)
D=T/S;          % Calculated Diffusivity (Value = .021)

% Equations

EQ1=(w./(2.*D));
EQ2=(-X.*(sqrt(EQ1)));
EQ3=(exp(EQ2));
EQ4=((w.*TM)-I-EQ2);
EQ5=cos(EQ4);

% Equation at time t

h=b+A.*EQ3.*EQ5;

% Difference from center

h_diff = h-1.5;
```

```
% Plot
figure;
axes1 = axes('Parent',figure,'FontSize',16);
view(axes1,[-37.5 30]);
grid(axes1,'on');
meshc(X,TM,h),...
    xlabel('Distance from Creek (m)','Fontsize',24),...
    ylabel('Time (s)','Fontsize',24),...
    zlabel('Water Table Height (m)','Fontsize',24)

%% Section 4 U_Tide

% data

% data stream
cutoff = 4550;
j=0;
well_orig = pr(:,7);
well_NAN = well_orig;
for i=1:size(well_orig,1)
    if(well_orig(i)<cutoff)
        well_NAN(i)=0/0;
    else
        j=j+1;
        well_cut(j)=well_orig(i);
        tday_cut(j)=tday(i);
    end
end

npavg = 5;
dn=2;
nstart = npavg-dn;
nend = size(well_orig,1)-dn;
wellrunavg = well_orig;
cutoff_min = 4288;
for i=nstart:nend
    wellrunavg(i)=mean(well_orig(i-dn:i+dn));


    well_keep(i) = 0/0;

    if (wellrunavg(i)-well_orig(i))> 40
        if((wellrunavg(i)-well_orig(i))<cutoff_min)
            well_keep (i) = well_orig(i);
        end
    end
end
figure, plot(well_orig), hold on, plot(wellrunavg, 'r')
figure, plot(well_keep)

% Utide on original signal
coef1 = ut_solv(tday, well_orig, [], 32, 'auto', 'NodsatNone','White','OLS',
'LinCI');

% Utide on NAN signal
coef2 = ut_solv(tday, well_NAN, [], 32, 'auto', 'NodsatNone','White','OLS',
```

```
'LinCI');

% Utide on cut signal
coef3 = ut_solv(tday_cut, well_cut, [], 32, 'auto',
'NodsatNone','White','OLS', 'LinCI');

% Reconstruct

[sl_fit, ~ ] = ut_reconstr(tday,coef1);

%%

% data stream

cutoff1     = 4672;
cutoff2     = 4647
cutoff3     = 4560;
cutoff4     = 4590;
cutoff5     = 4677;
cutoff6     = 4665;
cutoff7     = 4607;
cutoff8     = 4549;
cutoff9     = 4491;
cutoff10     = 4434;
cutoff11    = 4366;
cutoff12    = 4453;
cutoff13    = 4386;
cutoff14    = 4484;
cutoff15    = 4562;
cutoff16    = 4474;
cutoff17    = 4418;
start1      = 1;
start2      = 1093;
start3      = 2776;
start4      = 5250;
start5      = 10233;
start6      = 12918;
start7      = 15700;
start8      = 18677;
start9      = 19727;
start10      = 21117;
start11     = 21261;
start12     = 21680;
start13     = 22459;
start14     = 23955;
start15     = 24760;
start16     = 26891;
start17     = 28236;
end1        = start2 - 1;
end2        = start3 - 1;
end3        = start4 - 1;
end4        = start5 - 1;
end5        = start6 - 1;
end6        = start7 - 1;
end7        = start8 - 1;
end8        = start9 - 1;
end9        = start10 - 1;
```

```
end10       = start11 - 1;
end11       = start12 - 1;
end12       = start13 - 1;
end13       = start14 - 1;
end14       = start15 - 1;
end15       = start16 - 1;
end16       = start17 - 1;
end17       = 29632;

j=0;
well_orig = pr(:,7);
well_NOT = well_orig;
for i=start1:end1
    if(well_orig(i)<cutoff1)
        well_NOT(i)=0/0;

    end
end
for i=start2:end2
    if(well_orig(i)<cutoff2)
        well_NOT(i)=0/0;

    end
end
for i=start3:end3
    if(well_orig(i)<cutoff3)
        well_NOT(i)=0/0;

    end
end
for i=start4:end4
    if(well_orig(i)<cutoff4)
        well_NOT(i)=0/0;

    end
end
for i=start5:end5
    if(well_orig(i)<cutoff5)
        well_NOT(i)=0/0;

    end
end
for i=start6:end6
    if(well_orig(i)<cutoff6)
        well_NOT(i)=0/0;

    end
end
for i=start7:end7
    if(well_orig(i)<cutoff7)
        well_NOT(i)=0/0;

    end
end
for i=start8:end8
    if(well_orig(i)<cutoff8)
        well_NOT(i)=0/0;
```

```
    end
end
for i=start9:end9
    if(well_orig(i)<cutoff9)
        well_NOT(i)=0/0;

    end
end
for i=start10:end10
    if(well_orig(i)<cutoff10)
        well_NOT(i)=0/0;

    end
end
for i=start11:end11
    if(well_orig(i)<cutoff11)
        well_NOT(i)=0/0;

    end
end
for i=start12:end12
    if(well_orig(i)<cutoff12)
        well_NOT(i)=0/0;

    end
end
for i=start13:end13
    if(well_orig(i)<cutoff13)
        well_NOT(i)=0/0;

    end
end
for i=start14:end14
    if(well_orig(i)<cutoff14)
        well_NOT(i)=0/0;

    end
end
for i=start15:end15
    if(well_orig(i)<cutoff15)
        well_NOT(i)=0/0;

    end
end
for i=start16:end16
    if(well_orig(i)<cutoff16)
        well_NOT(i)=0/0;

    end
end
for i=start17:end17
    if(well_orig(i)<cutoff17)
        well_NOT(i)=0/0;

    end
```

```
end

% Plot Well Not

coef1 = ut_solv(tday, well_NOT, [], 32, 'auto', 'NodsatNone','White','OLS',
'LinCI');

[sl_fit, ~ ] = ut_reconstr(tday,coef1);

% Replacing data below cutoff

% Variables used
    % well_orig = Same as orginial signal/pr(:,7) (Pa)
    % well_NOT  = Signal with various cutoffs through out entire signal
    %             (Pa)
    % sl_fit    = Reconstructed signal from ut_recontr scripts (same time
    %             frame as orginal signal (Pa))
    % tday      = Time (matlab time)

well_NONUM = well_NOT;
recon = sl_fit;
for i=1:size(well_orig,1)
if isnan(well_NONUM(i))
%     if(well_NONUM(i)==0/0)
        recon(i) = well_orig(i);
    end
end

figure;
plot(recon-well_orig)

% Plot the final result
figure1 = figure;
    plot(tday,recon-well_orig), hold on
    xlabel('Date'),...
    ylabel('Pressure (Pa)'),...
    datetick('x','mm/dd/yy','keeplimits','keepticks')
    xlim([min(tday) max(tday)])
```